THESIS FOR THE DEGREE OF DOCTOR OF PHILOSOPHY
IN
THERMO AND FLUID DYNAMICS

Flow over rough surfaces, and conjugate heat transfer, in engineering applications

BERCELAY NIEBLES ATENCIO

Department of Mechanics and Maritime Sciences
Division of Fluid Dynamics
CHALMERS UNIVERSITY OF TECHNOLOGY

Gothenburg, Sweden 2018

Flow over rough surfaces, and conjugate heat transfer, in engineering applications

BERCELAY NIEBLES ATENCIO

ISBN: 978-91-7597-838-3

Doktorsavhandlingar vid Chalmers tekniska högskola
Ny serie nr. 4519
ISSN 0346-718X

Department of Mechanics and Maritime Sciences
Division of Fluid Dynamics
Chalmers University of Technology
SE-412 96 Gothenburg
Sweden
Telephone: +46(0)31-772 1000

Flow over rough surfaces, and conjugate heat transfer, in engineering applications

BERCELAY NIEBLES ATENCIO

Department of Mechanics and Maritime Sciences

Division of Fluid Dynamics

Chalmers University of Technology

Abstract

Nowadays, energy efficiency is an important matter to take care of, since the traditional energy sources are running out. Therefore, research in all engineering fields (Mechanical Engineering included) is moving towards not only creating new sustainable and environmentally friendly applications and products, but also towards modifying the existing engineering applications to make them more efficient from the energy point of view. Two important subjects in Mechanical Engineering are sharing this common goal: Fluid Mechanics and Heat Transfer. This thesis shows the work that has been done in these two subjects, in different projects.

Part of this research is carried out in order to contribute to the current knowledge of the drag caused by the flow over any arbitrary rough surface, since this is not yet fully understood. The fuel consumption and emissions are affected in great manner by the drag that is caused by a rough hull in the naval industry, for example. Experiments using different techniques such as PIV and rotating disk are presented, together with numerical simulations using commercial CFD codes.

On the other hand, the efficiency of electric generators used in hydro-power is greatly affected by the dissipation of the heat that is generated during the operation of these machines. This efficiency can be improved if the manufactures of such machines are provided with more accurate tools for determining the cooling system that these machines require during their operation and this is only possible if the heat transfer processes in these machines are understood. This work presents CFD simulations and experiments to contribute to the better understanding of how heat transfer occurs during the operation of this machines. Conjugate and convective heat transfer simulations are presented with the use of an open source code. Experiments using a technique that is based on a heat-mass transfer analogy are also performed.

Keywords: Antifouling, Electric Generator, Skin-Friction Drag, Correlation, Convective Heat Transfer, Rotating Disk, Naphthalene Sublimation Technique, CFD, Roughness Function, Impinging Jet, Stator Channel, RANS, Ship Hull.

Acknowledgements

I would like to thank my supervisors Håkan Nilsson and Valery Chernoray, for giving me the opportunity to work on two very interesting projects. I have learned a lot during these years under their guidance and support. Thereafter, I would like to thank all colleagues, researchers and staff of the Fluid Dynamics division for contributing to a great working environment. I am grateful to my wife for her love and support and now I thank God for our daughter. She is the best gift that I have ever received. I am also grateful to my parents, siblings and family. They have always supported all my endeavors.

Part of this work has been funded by the EU FP7 Project "Low-toxic cost-efficient environment friendly antifouling materials" (BYEFOULING) under Grant Agreement no. 612717. Many people involved in this project were also supportive and much gratitude goes to them, especially those working for companies such as JOTUN and MARINTEK in Norway and OCAS in Belgium.

Another part of this work was carried out thanks to the support of the "Swedish Hydro-power Center", SVC. I gratefully acknowledge Prof. Urban Lundin and Dr. Daniel Rundström, from Uppsala University and Voith Hydro AB, respectively, for providing their experience, advice and some useful information for running the simulations. The simulations were performed on resources provided by the Swedish National Infrastructure for Computing (SNIC).

List of Publications

This thesis is based on the work contained in the following papers:

I. Niebles Atencio B., Tokarev M., Chernoray V., (2016). "Submicron Resolution Long-Distance Micro-PIV Measurements in a Rough-Wall Boundary Layer" 18th International Symposium on the Application of Laser and Imaging Techniques to Fluid Mechanics, Lisbon.

II. Niebles Atencio B., Chernoray V., (2016). "A Resolved RANS CFD Approach for Drag Characterization of Antifouling Paints". Ocean Engineering. In Press

III. Niebles Atencio B., Nilsson H., (2018). "Evaluation of convective heat transfer correlations for network modelling of electric generator stator channels, based on conjugate and convective heat transfer CFD simulations". Paper to be submitted for publication.

IV. Niebles Atencio B, Jamshidi H, Liljemark M, Nilsson H, Chernoray V., (2018). "Assessment of the Naphthalene Sublimation Technique for Determination of Convective Heat Transfer in Fundamental and Industrial Applications". Paper to be submitted for publication.

Other Relevant Publications

Niebles Atencio B., Chernoray V., (2016). "Measurements and Prediction of Friction Drag of Hull Coatings". Paper in proceedings of 2nd Hull Performance & Insight Conference (HullPIC), 2016.

Romans 8:38-39 "For I am sure that neither death nor life, nor angels nor rulers, nor things present nor things to come, nor powers, nor height nor depth, nor anything else in all creation, will be able to separate us from the love of God in Christ Jesus our Lord."

Contents

Part A
Extended Summary

This thesis focuses on two important topics in the field of fluid mechanics and heat transfer that were treated separately. On the one hand, the flow over rough surfaces, which is not yet completely understood, despite of the fact that it has an important implication in many engineering applications, especially in the naval industry for ships and boats because the friction drag caused by fouling, antifouling coatings and roughness in general impacts the fuel consumption and toxic emissions to the atmosphere. In this thesis, new ways to measure and predict the friction drag of rough surfaces are presented, using both numerical simulations and experimental techniques.

On the other hand, conjugate heat transfer processes are also important in many applications, but a very relevant one is the electric generators for hydropower, since there is a current need of increasing the efficiency of these machines, which depends a lot on how they are cooled and therefore, on the rate at which the heat that is generated during their operation is dissipated (transferred to the cooling fluid). In this thesis, an experimental method for studying the heat transfer in these machines is presented and validated. Also, new correlations to improve the design phase of the electric generators are also developed.

The thesis consists of two parts: an extended summary and appended papers. In the extended summary part, the introduction presents relevant background and theory to get in context of the current situation of the engineering applications that have been previously described. Then the methodology that has been used for the CFD modelling and the experiments is presented. Next, the summary of the papers with some of the results are shown, followed by general concluding remarks. Finally, in part II of this thesis, the appended papers are presented.

1. Introduction

In the following, a description of the current situation regarding the engineering applications that are treated in this thesis is presented, together with relevant theory and information.

1.1. Friction Drag by Rough Surfaces

Marine transportation is a necessity for worldwide business activities. In 2016, total volumes of 10.3 billion tons of goods were loaded and transported by sea, with an increment of 2.6% from what was observed in 2015, and the forecast for 2017 was the total volumes reaching 10.6 billion tons of goods (UNCTAD, 2017). Owing to this increased transportation of goods, the environmental impacts of this activity are becoming increasingly important.

The condition of the surface of the hull of ships and boats plays an important role in the magnitude of frictional resistance. The frictional resistance is induced by the frictional forces around the hull surface of a ship. An emerging problem is to protect the hull of ships from the growth of a vast range of marine organisms (fouling), because a hull surface that has become rough due to the growth of algae, bacteria and barnacles may increase the ship's resistance up to 40% (Taylan, 2010). Other studies found increments up to 80% in the resistance due to fouling of hull and propeller (Munk, 2006). The immediate consequence of the increased resistance is an increment of the fuel consumption and greenhouse gas emissions. Therefore, in the naval architecture field, the effect of roughness is desirable to be fully understood. At present, a roughness allowance is calculated and added to frictional and residual coefficients when determining the overall drag of a full-scale ship (ITTC, 1978). Towsin et al. (1981) wanted to predict the roughness penalty more accurately and came up with a formulation based on the mean hull roughness and the Reynolds number, but representing the mean roughness over the hull of ships and boats is quite challenging. As it is well known, two of the major contributors to the surface roughness of a ship are the hull coating and the fouling. Antifouling coatings have been developed and used to counteract the effect of fouling on ships and boats, but a desirable characteristic of a good antifouling coating is of course, a low contribution to drag. Many researchers (eg Candries & Atlar, 2003) have studied the effect of antifouling coatings on the vessel drag but there is no common agreement on this topic.

Despite of the efforts in understanding the roughness effect on drag over vessels, due to the lack of more studies and methods to determine accurately the texture characteristics of rough surfaces, the ITTC Specialist Committee on Powering Performance Prediction concluded that there are reasons for questioning the accuracy of the currently used methods (ITTC, 2005). With this in mind, Flack and Schultz (2010) proposed a method to obtain equivalent sand-grain roughness height based on the root-mean-square of the roughness height and the skewness of

the roughness probability density function. Then, the frictional drag coefficient can be determined.

Characterizing the drag of a rough surface implies to find the velocity decrement caused by the frictional drag of the surface as a function of the roughness Reynolds number. This relationship is commonly known as a roughness function (Clauser, 1954 and Hama, 1954) and is unique for any particular surface roughness geometry. Once the roughness function for a given rough surface is known, it can be used in a numerical analysis to predict the drag of any body covered with that roughness.

1.1.1. Wall Roughness in Fluid Mechanics

Almost a century ago, Nikuradse (1933) carried out one of the most famous investigations regarding the effect of wall roughness on turbulent flows using pipes with uniform sand coating of different sizes. In this case of homogeneous sand, the roughness effect on the boundary layer depended only on the average sand-grain height k_s. His work was extended by Colebrook (1939), who analysed the flow in commercial pipes and by Moody (1944), who related the pressure drop in a pipe to the relative roughness (ratio of roughness height to pipe diameter) and Reynolds number. He consolidated the results into a very useful diagram commonly employed as engineering tool. Results by Allen et al. (2005) show that the pressure drop in the Moody diagram is overestimated in transitionally rough regimes for honed and commercial steel pipes. This clearly indicates that the Colebrook roughness function used in the formulation of Moody diagram may not be applicable to a wide range of roughness of engineering interest, according to Flack & Schultz (2010).

One of the big questions is whether the condition of the surface has any effect on the turbulent boundary layer mean flow and turbulence structure. Clauser (1954) and Hama (1954) introduced the roughness function concept. They found that the effect of surface roughness on the mean flow was limited to the inner layer, causing a downward shift in the log-law called the roughness function, ΔU^+.

Raupach et al. (1991) concluded that there is strong experimental support of outer-layer similarity in the turbulence structure over smooth and rough walls with regular roughness. This is termed the ‘wall similarity’ hypothesis, and it states that at sufficiently high Reynolds number, turbulent structures are independent of wall roughness and viscosity outside the roughness sublayer (or viscous sublayer in the case of a smooth wall), being the roughness

sublayer the region directly above the roughness, extending about 5k from the wall (where k is the roughness height) in which the turbulent motions are directly influenced by the roughness length scales. Moreover, experimental studies of Kunkel & Marusic (2006) and Flack et al. (2005), provided also support for wall similarity in smooth- and rough-wall boundary layer in terms of both the mean flow and the Reynolds stresses.

Jiménez (2004) stated that the conflicting views regarding the validity of the wall similarity hypothesis may be due to the effect of the relative roughness, k/δ, on the flow (where δ is the boundary-layer thickness). Jiménez concluded that if the roughness height is small compared to the boundary-layer thickness ($k/\delta < 1/40$), the effect of the roughness should be confined to the inner layer and wall similarity will hold. If, on the other hand, the roughness height is large compared to the boundary layer thickness ($k/\delta > 1/40$), roughness effects on the turbulence may extend across the entire boundary layer, and the concept of wall similarity will be invalid. Jimenez also notes that the classical notion of wall similarity has implications far beyond roughness studies, extending to the fundamental concepts of turbulence modelling. For example, the base of large-eddy simulation (LES) is that the small turbulence scales have little influence on the large energy-containing scales. If surface roughness exerts an influence across the entire boundary layer, this may not be a valid assumption. Krogstad and Efros (2012) performed experiments with squared bars and circular rods as roughness elements and found that the scale ratio proposed by Jimenez should be higher for the wall similarity hypothesis to hold.

Some researchers show their attempts in using the computational fluid dynamics to understand the effect of roughness on the turbulent structures and statistics in the turbulent boundary layers. Numerical simulations of turbulent channel flow by Leonardi et al. (2003) show roughness effect in the outer layer. Ashrafian et al. (2004) performed DNS simulations of turbulent flow in a rod-roughened channel and found significant differences in the turbulence field between smooth and rough wall boundary layers. Bhaganagar et al. (2004), concluded (using a 3D “egg carton” pattern roughness) that the streamwise and spanwise dimensions of roughness elements of fixed height play a crucial role in determining whether the roughness affects the outer layer. Another paper showing DNS studies on 3D and 2D roughness was presented by Lee et al (2011), who corroborated that the wall similarity did not hold in the outer layer. However, in his paper a possible explanation for a failed wall similarity case could be related to the arrangement of the roughness elements.

It is worth to note that numerical and experimental studies of roughness effects and the determination of roughness function have been usually conducted on regular and uniform distribution of roughness elements and shapes, as mentioned by Yuan & Piomelli (2014), who performed LES simulations to determine roughness function and equivalent sand-grain roughness height of realistic roughness replicated from hydraulic turbines. They found k_s depending strongly on the topography of the surface and moments of surface height statistics not predicting the roughness function as good as the predictions of the correlations based on slope parameters. This method, is however, very computationally expensive and therefore, we are proposing a new approach in this study.

1.1.2. The Roughness Function

The classical log-law of the mean velocity profile in the inner part of a turbulent boundary layer can be expressed as:

$$U^+ = \frac{1}{\kappa} \ln(y^+) + B \tag{1}$$

where U^+ is the inner boundary layer velocity, κ is the von Kármán constant, y^+ is the normalized distance from the wall and B is the smooth-wall log-law intercept. Classical values for the pipe flow used since the early 1900s are κ = 0.4 and B = 5.5 (Schlichting, 1979) and for the flat plate boundary layer κ = 0.39 and B = 5.56 (Schlichting, 1979).

The effect of the surface roughness is to shift the velocity profile in the log-law layer downwards as a consequence of the increase in frictional drag on the surface. This downward shift is called the roughness function, ΔU^+(see Figure 1). The modified law of the wall with the roughness function term reads

$$U^+ = \frac{1}{\kappa} \ln(y^+) + B - \Delta U^+ \tag{2}$$

ΔU^+ depends on the roughness Reynolds number, k^+, defined as the ratio of the roughness length scale k to the viscous length scale ν/U_τ, which is based on the kinematic viscosity ν, and the friction velocity, $U_\tau = \sqrt{\tau_0/\rho}$.

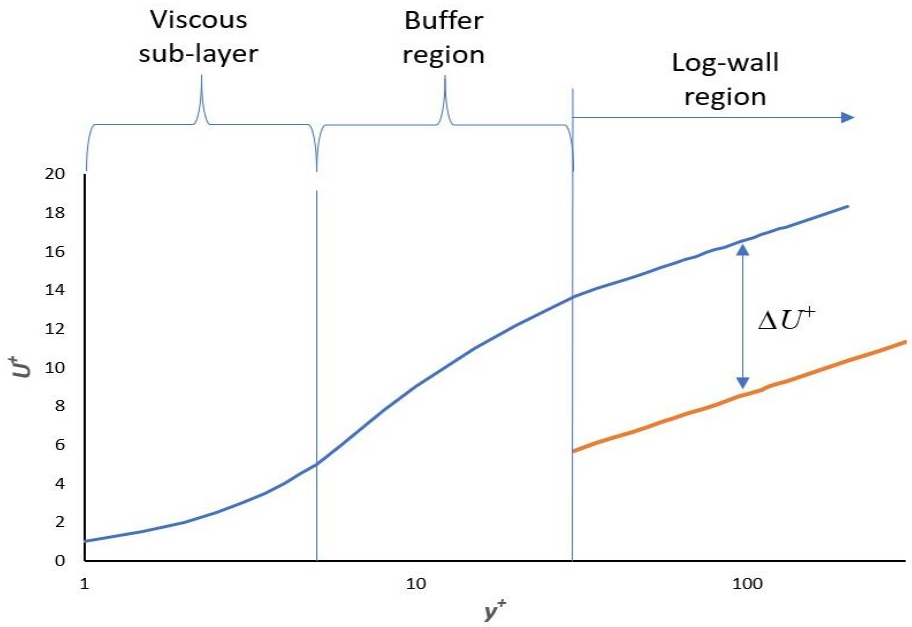

Figure 1. Boundary layer velocity profile and the roughness function.

It is customary to define the roughness height in terms of the equivalent sand-grain roughness height, k_s ; the corresponding Reynolds number based on the equivalent sand-grain roughness height would then be

$$k_s{}^+ = \frac{k_s\, U_\tau}{\nu} \tag{3}$$

Nikuradse (1933) found that, at $k_s{}^+ < 2 - 5$, the surface behaves like a smooth surface and, at $k_s{}^+ >$ 60-90, the so-called completely rough regime is established, so that the resistance factor is independent of the Reynolds number. He called the regime between these two, the transitional regime.

Hama (1954) showed that, from the wall law and the velocity defect law, one can express the roughness function as

$$\Delta U^+ = \left(\sqrt{\frac{2}{c_f}}\right)_s - \left(\sqrt{\frac{2}{c_f}}\right)_r \tag{4}$$

where c_f is the skin friction coefficient and the subscripts s and r refer to smooth and rough surface, respectively. This relation directly indicates the importance of the parameter ΔU^+ and eliminates the need of velocity profiles to find the velocity defect that owes to roughness.

Granville (1987) showed that a similar expression is valid for fully developed pipe and channel flows

$$\Delta U^+ = \left(\sqrt{\frac{2}{f}}\right)_s - \left(\sqrt{\frac{2}{f}}\right)_r \tag{5}$$

where the Fanning friction factor, f, is used rather than c_f and is defined as (Darcy friction factor, $\lambda = 4f$)

$$f = \frac{2\tau_0}{\rho \overline{U}^2} \tag{6}$$

and τ_0 is the wall shear stress while $\overline{U}$ is the bulk velocity. The derivation requires that the values of the Fanning friction factor f for smooth and rough surfaces in Equation 6 should be taken at the same $Re_h\sqrt{f}$, where Re_h is the Reynolds number based on channel height or pipe diameter.

1.1.3. Rotating Disk Flow

The boundary layer that is formed on the disk surface is three-dimensional due to a cross-flow velocity component, which is also named as a radial velocity. Schlichting (1979), explains that due to friction, the fluid which is adjacent to the disk is carried by it and then, the centrifugal acceleration forces the fluid outwards, creating radial and tangential components (V_r and V_ϕ in Figure 2). The mass of fluid that has been driven outwards by the action of the centrifugal force is replaced by an axially flowing fluid with velocity V_z.

The flow Reynolds number in this case is defined as

$$Re_r = V\frac{r}{\nu} \tag{7}$$

where r denotes the disk radius and $V = \omega r$ is the velocity at the tip of the disk, with ω as the angular velocity.

Another important dimensionless parameter is the moment or torque coefficient C_m, which is defined by Granville (1982) as

$$C_m = \frac{4M}{\rho r_d{}^5 (\phi\omega)^2} \tag{8}$$

where M is the torque from one side of the disk and ϕ is a swirl factor (defined $\phi^2 = C_{m,en}/C_{m,\infty}$ and normal values, $0 < \phi < 1$) that accounts for the swirl that may develop in enclosed rotating disk flows, reducing the effective angular velocity.

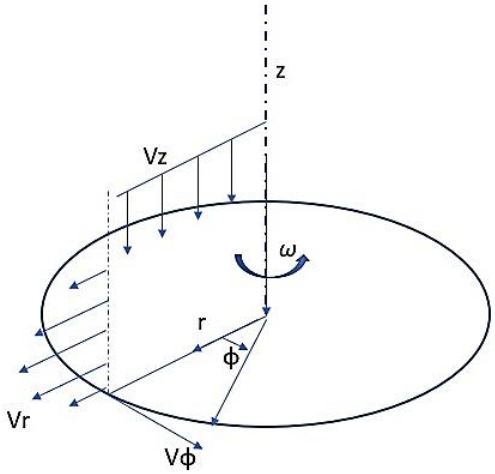

Figure 2. Schematic of velocity components on rotating disks.

In the boundary layer that is developed on the disc, V_z is small and V_ϕ is an order of magnitude larger than V_r and therefore, it is the dominant velocity component and also considered to obey the law of the wall (Granville, 1982).

Granville (1972) observed that transition from laminar to turbulent for smooth disks occur at $Re_r = 2.9 \times 10^5$ and that a correction in the torque coefficient is required for the presence of laminar flow in part of the disk. However, as he also observed, the correction is smaller as Re_r increases and the effect in the torque is negligible. This can be also confirmed in the work performed in this thesis. If the definition of the dimensionless radial coordinate $Ra = r(\omega/\nu)^{0.5}$, is used, the radius at which transition from laminar to turbulent occurs can be estimated using Ra = 510 as used by Imayama et al. (2016). Depending on the rotational speed, the transition in the cases investigated in this thesis is always located in the region r = 0.063-0.076 m. For a disk with total radius of 0.15 m, the transition region is then located around half the radius. Finding the location of transition is important to understand how the laminar part of the rotating disk flow affects the torque. From the definition of the skin friction coefficient, it is possible to obtain the local wall shear stress at any radius and any rotational velocity. The wall shear stress

in terms of the skin friction coefficient can be used in the definition of torque (force × distance). Therefore, the wall shear stress and torque can be expressed, respectively, as

$$\tau_w = c_f \frac{\rho u^2}{2} \tag{9}$$

and

$$T = \int_0^{r_0} \left(c_f \frac{\rho u^2}{2} \right) 2\pi r \cdot r \cdot dr \tag{10}$$

A ratio between half of the torque (integrating from $r_0/2$ to r_0) to the total torque (integrating from 0 to r_0) can be obtained if, for simplicity in the calculations, the local skin friction is assumed to follow Prandtl's equation, which for the case of a disk reads

$$c_f{}^{0.5} = \frac{Re_r{}^{0.1}}{0.0576^{0.5}} \tag{11}$$

By calculating the ratio of the torques that results from integrating Equation 10, the part of the disk from half of the radius to the edge is found to contribute to around 95% of the surface torque. This means that the region from which the flow of the rotating disk starts becoming turbulent contributes to 95% of the torque and the laminar part of the disk flow contributes to 5%.

The effect of the edge has been also considered before. Granville (1982) showed that the wall shear stress coefficient at the disk edge is close in value to the average coefficient in both smooth and rough disks. Granville (1972) reported that the effect of the edge on the torque is around 4%. The edge of the disk has an effect on the total torque and complex secondary flow with vortices are found in this area. However, the edge effect on the boundary layer over the rotating disk seems to be negligible.

In the cases of rough disks, the roughness function expression was derived by Granville (1982), which reads

$$\Delta U^+ = \sqrt{\frac{8\pi}{5}} \left[\left(\frac{1}{\sqrt{C_m}} \right)_s - \left(\frac{1}{\sqrt{C_m}} \right)_r \right] + \frac{1}{5} (\Delta U^+)' \tag{12a}$$

$$(\Delta U^+)' = \frac{d(\Delta U^+)}{d(\ln U_\tau)} \tag{12b}$$

where the subscripts *s* and *r* are referred to smooth and rough surfaces, respectively. The process of determining the roughness function, as can be seen from equations 12a and 12b, does not depend on the roughness Reynolds number along the disk radius.

1.1.4. Particle Image Velocimetry (PIV)

Particle Image Velocimetry (PIV) indirectly measures flow velocity, see Raffel et al. (2007). The displacement of particles immersed in fluid flow is recorded photographically and analysed. The PIV method is non-intrusive and allows to record the flow velocity without disturbing the flow. At least two consecutive images, with known time interval are required in order to determine the displacement of the particles. The velocity can be then calculated by computing the displacement of the particles over the given time interval.

Figure 3 illustrates the overall process in PIV. The displacement of particles is derived from analysing the intensity of image pairs using statistics based on specific areas of the image called interrogation windows. The particles used in PIV are called tracers and are critical in the PIV measurement since the fluid velocity is measured via the particle velocity. The first consideration when choosing the seeding particles is therefore visibility. The particles have to have a sufficient size and a good refractive index in order to achieve good scattering intensity. The size of the particles must be balanced with the fidelity of the particles following the flow. For acceptable tracing accuracy, the particle response time should be faster than the smallest time scale of the flow. The accuracy of the PIV measurement is therefore limited by the ability of the tracer particles to follow the fluid flow. The non-dimensional number that measures the faithfulness with which the particles follow the flow is the Stokes number (St), defined as the ratio of the response time of a particle to the response time of the flow. The conditions where $St < 0.1$ gives an acceptable flow tracing accuracy with errors less than 1%.

In order to find the particles displacement over a short period of time, two images that have been successively recorded are compared. A small sub-area of the first image (interrogation window), is compared with the second image interrogation window by using a cross-correlation technique, resulting in a velocity vector for that particular particle pattern. This evaluation

process is repeated for all interrogation windows of the pair of images and the final outcome is a complete vector diagram of the flow under study.

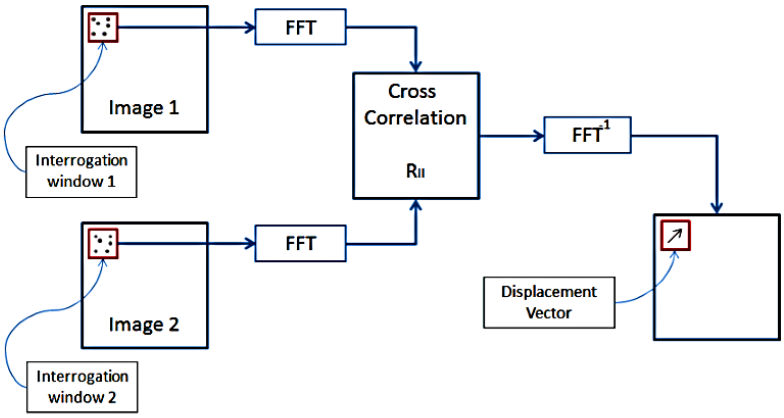

Figure 3. Flow chart of the processing algorithm in PIV.

1.2. Hydropower electric generators

Hydropower energy is the leading renewable source of electricity generation worldwide, taking care of the 71% of all renewable electricity and generating 16.4% of the world's electricity in 2016. Hydropower development has increased globally and in 10 years (from 2005 to 2015), the total installed capacity has grown by 39%, with an average growth rate of nearly 4% per year (World Energy Council, 2016).

Hydropower is based on the synergic work of a turbine and generator to convert hydraulic energy into electrical energy. The hydraulic energy created by the moving water spins the rotor of the turbine. The Dam Hydroelectricity production type is sketched in Figure 4 and utilizes the potential energy from dammed water for the production of electricity. The dam is a large barrier that forms a reservoir of water and its purpose is to raise the level of water and control its flow. The elevation of the dam creates gravitational force that turns the turbine when the water is released and passes by the turbine blades. This turbine is connected to an electromagnetic generator which produces electricity as the turbine spins.

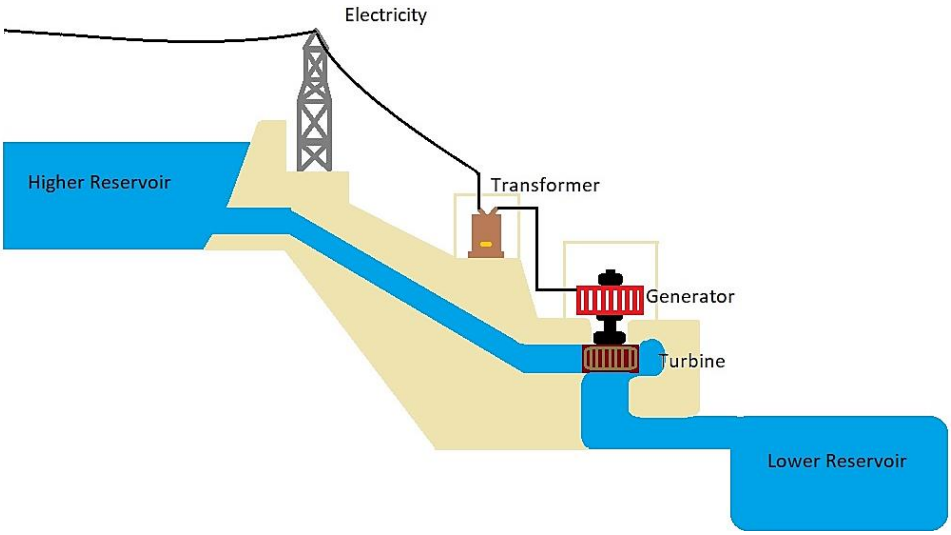

Figure 4. Cross-section of a conventional dam for hydroelectricity production.

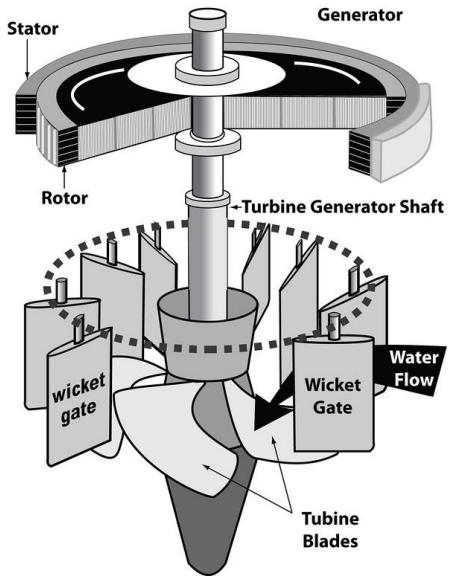

Figure 5. Electric generator and main components. Source: Need Media (2018).

An important player in hydropower is the electric generator, which is the machine that converts mechanical energy into electrical energy. For understanding how this conversion occurs, it is first necessary to identify the main components of a hydropower generator and their role. Figure 5 illustrates the main parts of a generator, which are basically the rotor and the stator. The rotor is the rotating component of the generator and receives its rotation from the turbine. It is composed by many electromagnetic poles, in which the electromagnetic field is constantly moving as the rotor spins. The rotor rotates inside of the static part of the generator, which is

called the stator. The stator is composed mainly of a core with ventilation channels and copper windings or coils that are excited when the electromagnetic field of the rotor poles passes by. Every complete turn of the rotor creates a pulse in the stator windings that is transmitted to conductors attached to the stator and then to the grid.

As in any other machine, the electric generator suffers from some losses that are present during its operation, which are generally classified in three groups (Moradnia and Nilsson, 2011): the electric losses are also known as copper losses and are caused by the electric currents passing through electric resistances, generating heat. The magnetic losses, also known as core or iron losses, are losses caused by the magnetic properties of the stator core when it is exposed to a magnetic field that changes direction continuously. The losses are created by the interaction of electrons. The mechanical losses are those caused by windage losses and friction losses. The former refers to the power lost due to the internal friction of the ventilation flow when it passes through the components of the cooling system. The friction losses are those occurring in bearings and brushes. The three groups of losses together contribute to an elevation of the temperature in the electric generators. The elevated temperature leads to increased electrical resistance, which in turn leads to increased losses. Additionally, an increased temperature in the electric generator might damage the insulation present in the stator and the rotor. It is thus crucial to keep the operating temperature of the generator within working range to optimize generators performance and durability. The spatial and temporal variations of the temperature should as well be kept to a minimum to avoid thermal stresses that deteriorate the materials.

The present thesis is devoted to axially cooled electric generators and Figure 6 shows a schematic of the cooling flow in axially cooled generators. Axially cooled generators are normally equipped with axial fans at each end to supply the cooling air. The air flows axially through the spaces in between the poles and the rotor-stator air gap. The rotor induces a tangential flow component, and the air then enters the ventilation channels of the stator to remove heat from the electric windings and the iron core. Finally, the air is cooled down by heat exchangers and redirected to the fans to start the cycle again.

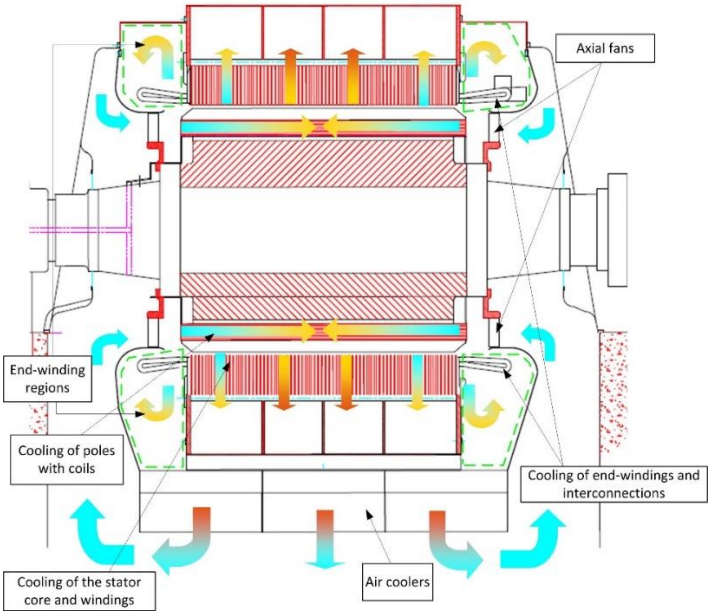

Figure 6. Flow of air in axially cooled generators. Source: Voith Hydro AB.

Despite of being a large contribution of the total generator losses and its relevance for an efficient generation of electricity and for the durability of the generator itself, the cooling in electric generators has received little attention, but there are recent studies in the literature that try to fill the knowledge gap in this field. Pickering et al. (2001), used a commercial CFD code to predict the air flow and heat transfer on the rotor of a salient pole machine and found agreement with experiments. Fujita et al. (2005), introduced a multi-pitched ventilation channel system in the stator core of air-cooled generators to reduce the windage losses and examined an optimal design of ventilation channels for reducing also the current losses. Ujiie et al. (2006), applied a combination of scaled model test, network models and CFD to improve the air flow rate distribution in a large hydrogenator. Traxler-Samek et al. (2010), presented a method to calculate the airflow, losses and temperatures for large hydro-generators. The result is an overview of the temperature gradients for fine tuning the cooling airflow. Pasha et al. (2010) described an upgrading for a large hydro-generator and studied the windage losses and pressure losses by experiments and CFD. Moradnia (2013), used a fully predictive approach to carry out a number of parametric studies on the rotor and stator geometries to understand how to increase the volume flow rate through the machine. In another study Moradnia et al. (2014) described experimental and numerical studies on a half scale model of an electrical generator to investigate in detail the flow of air through the machine, as a first step towards accurate heat transfer analysis. Bin et al. (2014), used CFD and heat transfer theory to discuss the cooling capacity of a 150-MW air-cooled generator and found that the height of the radial ventilation

channel, the material of the cross-bow support components and geometry of support components can lead to decrease in stator temperatures. Schrittwieser et al. (2014), used a commercial CFD software to analyse the fluid flow in the stator channels of hydrogenerators to define simplifications that could be allowed for accelerating the simulations. In another study, Schrittwieser et al. (2015), trained and validated a neural network and were able to compute the heat transfer coefficients, both for the yoke and tooth region of the stator ventilation channel of large air-cooled machines using different input parameters. Jamshidi et al. (2014, 2017) and Jamshidi (2017) presented experimental and numerical studies of the ventilation flow inside hydro-generators with extensive results to understand the flow distribution inside the stator ventilation channels at different operational conditions and geometrical configurations. The knowledge that has been gained from previous studies can be used to improve the design phase of the cooling systems in hydro-generators.

1.2.1. Network Models for the Design of Electric Generators

The design of hydro-generators relies on network model methods (also called analytical), which have been established for thermal and flow calculations (Traxler-Samek et al., 2010). Extensive studies have been developed to analyse the pros and cons of using network models for designing these machines and Boglietti et al. (2009) presented one of such studies. He points out the need of performing deeper thermal analysis studies to aid in a better design of these machines and compares the thermal analysis that can be done by using network models with those that can be obtained by FEM and CFD.

The analytical method uses lumped parameter networks for combining flow and thermal networks that are fast to solve and modify, but with some drawbacks such as being difficult to build and calibrate. As the name suggests, the network model is a circuit of discrete elements that simplify and represent systems and complex geometries. The purpose of the thermal network is to calculate the temperature of the elements and the heat transfer among them. The fluid network allows the determination of volume flow in each flow path. In Figure 7, a part of a thermal model layout is shown. Here, temperature of a node (in green) is calculated based on operations among the inputs (initial temperature values).

Few examples of the research that has been done in network models are now presented. One of the oldest works is the general method for performing a flow network analysis on a ventilated electrical machine reported by Taylor (1960). Another pioneer work is the one by Mellor et al.

(1991), which was one of the first to describe a lumped thermal network for the thermal model of a totally enclosed fan cooled induction motors. The electrical machine was reduced to a number of discrete elements under the assumption of negligible temperature difference inside each element by using conduction, convection and radiation thermal resistances, so that the heat flow was able to be modelled. Bumby and Martin (2005) used a simple network for modelling the stator section and calculated the maximum temperature in the copper windings for a particular generator design. Hodgins et al. (2012) presented a modular air-cored linear PM generator that could be used for wave energy and used a lumped thermal network for the design of a 50-kW linear generator prototype.

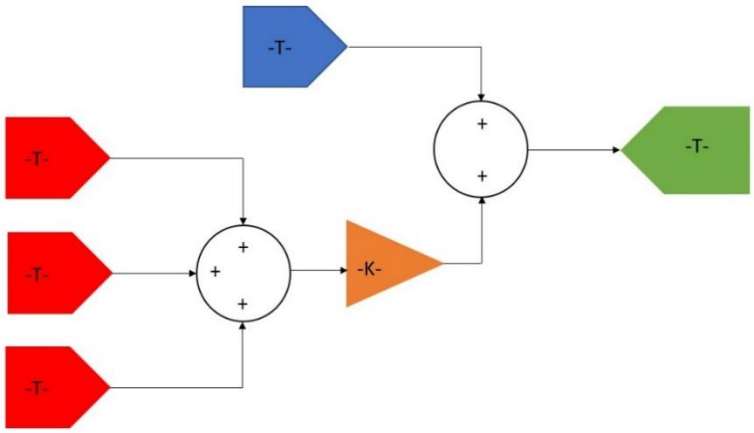

Figure 7. Example of a thermal model layout.

Many other researchers have also revised the applicability of the lumped networks for the design of electrical machines and have proposed their own methods to build them. When it comes to electrical machine manufacturers, they have also developed their own codes to be used during the design phase of their products. Some of these codes are confidential and only used by the company, while some other codes have been developed for commercial purposes. Cabré Gimeno (2017) reported an example of a network model that has been built with MATLAB and Simulink. This model uses the lumped element method for both the flow and thermal analysis in a hydro-generator. In his work, the fluid network is based on the friction resistance and pressure drop of the air as it passes through ducts and the different parts of the generator. For thermal analysis, the geometry is discretized into nodes with defined sizes and physical properties depending on the node material are assigned to them. Thermal resistances are then calculated using heat transfer theory and equations. By using heat transfer correlations,

the temperatures of the air in the ventilation channel and the temperatures of the different stator components are determined.

Figure 8 shows the flow of information from the fluid to the thermal networks in the example of a network model presented by Cabré Gimeno (2017). In this work, the outputs of the fluid model are inputs for the thermal model. The fluid network calculates the air flow in each channel and this airflow is used for determining the heat transfer coefficients. Then, airflow, heat transfer coefficients and losses are used as input of the thermal model to calculate the different output temperatures of the components of the generator.

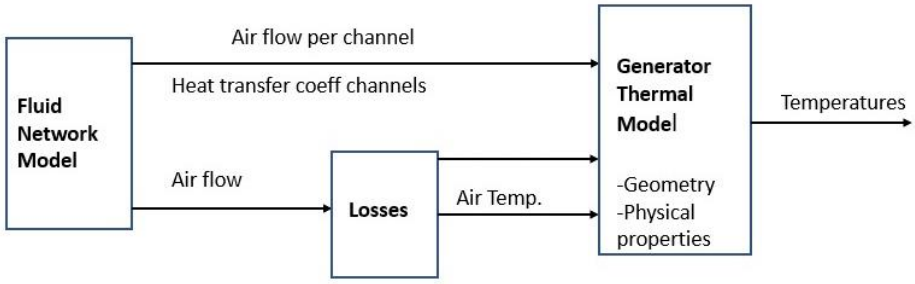

Figure 8. Flow of information from the fluid network to the thermal network in the model by Cabré Gimeno (2017).

1.2.2. Heat Transfer and Experimental Correlations

As previously mentioned, the network models rely on the use of experimental correlations for calculating the heat transfer coefficients for estimating temperatures, which in turn, are used for designing and dimensioning of the cooling system of the hydro-generator. Therefore, a more accurate estimation of the heat transfer in the generators will lead to better design of cooling systems to help increase the overall efficiency of the machine, as discussed in Section 1.2.

Previous investigations by Moradnia (2013) and Jamshidi (2017) show that the flow inside the ventilation channels of the stator in electrical generators is not evenly distributed among the different ventilation channel rows. The flow is not uniform in each channel and is affected by both tangential and axial components of velocity in the rotor-stator gap. The flow is far from a fully-developed channel flow and is associated with large recirculation regions due to flow separations. These flow characteristics are far from those used to determine heat transfer correlations which are currently used for the thermal analysis of the stator ventilation channels in electrical generators.

For understanding the heat transfer correlations that can be found in the literature and are used by the network models, it is first important to briefly clarify some basics concepts. First of all, the common definition of "heat transfer" is the transit of thermal energy due to a spatial temperature difference (Incropera et al. 2013). Different types of heat transfer processes or modes are normally found in engineering applications but in this thesis the focus is on the following two modes:

Conduction: refers to the heat transfer that occurs across a stationary medium, which can be a solid or a fluid. The Fourier law governs this type of heat transfer. The Fourier law reads

$$q_x = -kA\nabla T, \tag{13}$$

where q_x is the heat transfer by conduction in the x-direction across the medium, k is a transport property of the medium known as thermal conductivity, A is the cross-sectional area through which the heat is transported and ∇T denotes a temperature gradient in the x-direction.

Convection: the heat q is transferred by molecular diffusion and motion of the fluid over a surface. It is expressed as

$$q = hA(T_s - T_\infty). \tag{14}$$

In this case, the difference in temperature occurs between the surface (T_s) and the free-stream fluid (T_∞) and h is called the convection coefficient. The third heat transfer mode is radiation, which is not considered in this thesis due to the very small contribution to the overall heat transfer.

For convective heat transfer, an important dimensionless parameter is the Nusselt number (Nu) which expresses the ratio of convection to pure conduction for a body with a characteristic length L. Nu is defined as

$$Nu = \frac{hL}{k} \tag{15}$$

Another dimensionless parameter is the Reynolds number Re, which expresses the ratio of the inertial to viscous forces acting on a fluid element and based on this, determine whether the flow is laminar or turbulent. The definition of Re is as follows

$$Re = \frac{UL}{\nu} \tag{16}$$

where U is a characteristic velocity of the fluid and ν is the kinematic viscosity.

Finally, the ratio of momentum to thermal diffusion (the latter expressed by the thermal diffusivity, α) is known as the Prandtl number, Pr, and its definition is

$$Pr = \frac{\nu}{\alpha} \tag{17}$$

In the following, some of the most known heat transfer correlations are shown. The correlations normally relate the Nusselt number with other dimensionless groups such as Prandtl and Reynolds numbers. Some works and investigations have been based on these correlations. Mejuto (2010) used an average of the Dittus - Boelter correlation and the Gnielinksi correlation for the thermal modelling of synchronous generators. For circular ducts, the widely known correlation by Dittus and Boelter (1930) reads

$$Nu = 0.023 Re^{0.8} Pr^{0.4} \tag{18}$$

In Equation 18, Re is based on the diameter of the pipe and fluid properties are evaluated at the bulk temperature. This correlation has been obtained for fully turbulent flows ($Re \geq 10000$) and for $0.6 \leq Pr \leq 160$ and it is widely used, since only knowledge of the bulk temperature is required for using it. However, Jo et al (2014) recommends only Dittus - Boelter equation for the cases when the difference between the wall and coolant temperatures is rather small. Dittus-Boelter correlation is only useful as a rough estimate of the heat transfer in pipes, since errors as large as 25% may result from using it (Incropera et al., 2013).

More recent and complex correlations have been developed and one example is the one by Gnielinksi (1979) which reads

$$Nu = \frac{(f/8)\,(Re - 1000)Pr}{1 + 12.7\,(f/8)^{1/2}\,(Pr^{2/3} - 1)} \tag{19}$$

Less errors (close to 10%) can be obtained with Equation 19 (Incropera et al., 2013) and the application is valid for a wide range of Reynolds numbers, but requires the additional

information of the friction factor f, which can be obtained from the Moody diagram or correlations.

1.2.3. The Naphthalene Sublimation Technique

The naphthalene sublimation technique is an experimental technique that has been used to determine the heat transfer coefficients for convective flows**.** The basis for using the naphthalene sublimation technique rests on the analogy between heat and mass transfer processes. Mass transfer experiments are performed and then heat transfer results are determined by using the concept of heat and mass transfer analogy.

The naphthalene sublimation technique is particularly useful in complex flows and complex geometries with restrictions in the visual access. In heat transfer measurements, large gradients in transfer rate are commonly difficult to capture, but they can be determined even at corners and edges with the naphthalene sublimation technique. Boundary conditions for mass transfer that are analogous to isothermal and adiabatic walls in convective heat transfer can be easily imposed with this method. The surface that is coated or made of naphthalene acts as an isothermal surface while the other surfaces are adiabatic.

The heat transfer coefficient can be readily determined via the mass/heat transfer analogy from the measured mass transfer which is as follows

$$\frac{Nu}{Sh} = \left(\frac{Pr}{Sc}\right)^{n} \tag{20}$$

where Sh and Sc are the Sherwood and Schmidt numbers, respectively. The value of n can be 0.3 or 0.4 for external or internal flows, respectively (Souza Mendes, 1991).

1.3. Scope of the thesis

The scope of the work presented in this thesis is described separately for the two engineering applications that are considered.

1.3.1. Friction Drag by Rough Surfaces

The work in this case is focused on developing methods to evaluate the frictional drag caused by antifouling paints, but this could be applied in general to any arbitrary rough surface. For this purpose, a rotating disk rig has been designed and built. Rotating disks that have been coated with antifouling coatings are provided. Rotating disks with sandpaper are also to be used for the experiments. Some experimental techniques were evaluated, and torque measurements are decided to be used in a combination with particle image velocimetry. The experiments are thus, based on these two experimental techniques. Flat plate experimental results provided by an external partner are also used for comparison.

Regarding the numerical simulations, the work is focused on running simulations using a commercial CFD code for a channel with walls with similar roughness as those of the disks.

1.3.2. Hydropower electric generators

The aim in this case is to provide experimental data for validation of heat transfer in the stator channels of a generator in a model that was built for previous studies on the cooling air flow. The experiments are based only on the naphthalene sublimation technique and their results are compared with CFD simulations performed using an open source code.

Conjugate heat transfer CFD simulations are performed in order to develop a new correlation that could be used during the design phase of electric generators to increase the efficiency of these machines in hydropower applications. These simulations are also based on an open source code. The resulting correlation is used in an existing network model and the results from using it, compared with results from another correlation that is normally used in network models.

2. CFD Modeling

This chapter will describe the CFD methodology that has been followed to carry out the work that is presented in this thesis. The methodology is discussed separately for both engineering applications.

2.1. Friction Drag by Rough Surfaces

This section describes the governing equations, geometries, mesh generation and some numerical aspects related to the CFD modelling of flow over rough surfaces.

2.1.1. Governing Equations

The steady and unsteady implementation of Reynolds-Averaged Navier-Stokes equations were used to solve the governing flow equations (mass and momentum conservation). The CFD commercial software for this purpose was Star-CCM+ v 9.06.009.

For incompressible flows, the averaged continuity and momentum equations are described by the following expressions (Ferziger and Peric, 2002):

$$\frac{\partial \bar{u}_i}{\partial x_i} = 0 \tag{21}$$

$$\frac{\partial}{\partial x_j}\left(\bar{u}_i\bar{u}_j + \overline{u_i'u_j'}\right) = -\frac{1}{\rho}\frac{\partial \bar{p}}{\partial x_i} + \frac{\partial \bar{\tau}_{ij}}{\partial x_j} \tag{22}$$

In these equations, ρ is the density, $\bar{u}_i$ is the Cartesian components of the vector of average velocity, $\overline{u_i'u_j'}$ is the Reynolds stresses and $\bar{p}$ is the mean pressure. $\bar{\tau}_{ij}$ represents the tensor components of the mean viscous stress, as follows:

$$\bar{\tau}_{ij} = \nu\left(\frac{\partial \bar{u}_i}{\partial x_j} + \frac{\partial \bar{u}_j}{\partial x_i}\right) \tag{23}$$

where $\nu = \mu/\rho$ is the kinematic viscosity.

The Reynolds stresses need to be modelled and therefore, the Boussinesq assumption is required (Boussinesq, 1877).

2.1.2. Geometry, mesh generation and boundary conditions

Two different types of domains with roughness were used for the simulations: periodic roughness and arbitrary roughness of antifouling paints. Figure 9 shows a lateral view of the first domain type. A 3D channel with height h=0.01 m and a bottom wall with an area of 5 mm × 20 mm is used. The bottom wall had also a protuberance or step that represented the periodic roughness. The height of the step is 0.5 mm. The mesh was created in ICEM CFD and the refinement was on the bottom wall and the corners of the step.

Figure 9. Lateral view of the domain for the periodic roughness case.

The second type of roughness is the case of arbitrary roughness from antifouling paints. Three different rough surfaces were used in this case that corresponded to realistic surfaces of antifouling paints used in marine applications. Two most commonly used methods used for characterization of marine coatings are using a rotating disks apparatus and towing plates in a tank. Thus, for the experimental characterization of coatings, models of flat plates and disks were prepared, coated and scanned using 3D laser profilometry at Jotun A/S (Norway). The 3D profilometer surface scans of the disks were used as an input geometry for the resolved CFD calculations. A representative area of the entire scan was selected to be simulated for this reason. The scanned areas are 40 mm × 40 mm, but an area of 5 mm × 20 mm was used for the simulations. This simulated area should exhibit characteristics of the roughness presented in the entire disk.

Resulting data files with coordinates XYZ from the scanning of the disks were used in MATLAB to create surface profiles. These profiles were then converted into STL files that were imported by the mesh generator software, which in this case was ANSYS ICEM CFD.

Once in ICEM, the flow domain for the resolved CFD simulations was created as a channel with rough bottom wall. The height of the simulated channel was $2h$=0.02 m and the height of the domain was h=0.01 m (Figure 10). A grid sensitivity study and discretization errors where estimated for these cases of arbitrary roughness.

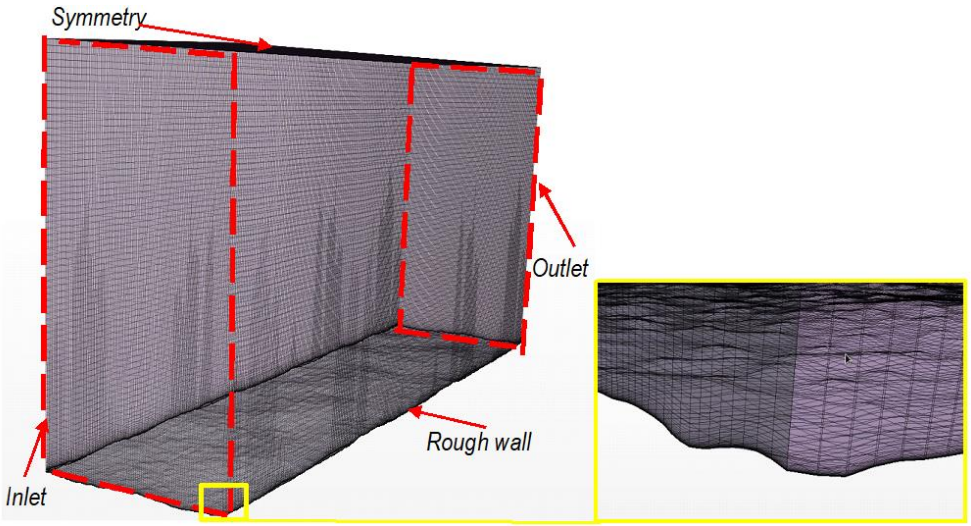

Figure 10. Computational mesh for case B and a zoomed view of the bottom rough wall.

For the periodic roughness cases, the bottom of the channel is a no-slip boundary. The top wall of the channel is a symmetry condition, the inlet, outlet and side wall boundaries, periodic conditions were set. The inlet velocities were the tangential velocities that could be obtained from a disk rotating at 300 and 600 rpm in the experiments (described later). The velocities thus, were 4.24 and 8.24 m/s.

For the cases with the antifouling coatings, the bottom of the channel (where the roughness is present) was set to be a no-slip boundary, whereas the top is a symmetric wall (slip) boundary. For the inlet, outlet and side wall boundaries, periodic conditions were set, and the mass flow was specified, which corresponded to Re_h of 84000 to 280000 (this velocity range includes the same inlet velocities as in the sand-paper cases).

2.1.3. Numerical aspects

Steady-state simulations were performed for the sand-paper and periodic roughness cases, whereas unsteady simulations for the case of antifouling coatings. Star-CCM+ uses a finite volume method to discretize the governing equations. For the momentum equations a second order convection scheme was used and for temporal discretization, a first order approximation

was used. The flow equations were solved in a segregated manner and a predictor-corrector approach was used for linking the continuity and momentum equations. The shear stress transport (SST) $k-\omega$ turbulence model was used for closing the RANS equations, blending the $k-\omega$ model near the wall and the $k-\varepsilon$ model in the far field. For the unsteady cases, a time step was used such that the Courant-Friedrichs-Lewis number (CFL) is kept as 1 or less.

2.2. Hydropower electric generators

This section describes the governing equations, geometries, mesh generation and some numerical aspects related to the work on cooling of hydropower generator.

2.2.1. Governing Equations

For the development of correlations for predicting the heat transfer in the stator channels of electric generators, conjugate heat transfer simulations are performed. Continuity and momentum equation are solved in the fluid region. The energy equation is solved in both the solid and fluid regions. The continuity and momentum equations for incompressible flow that will be solved in this case have been already shown by Equations 21-23. The heat equation reads as follows

$$\frac{\partial(u_i T)}{\partial t} = \frac{k_t}{\rho c_p}\frac{\partial^2 T}{\partial {x_i}^2} + q''' \tag{24}$$

where c_p is the heat capacity of the medium, T is its temperature, k_t is the thermal conductivity and q''' is a heat source term that is zero (0) for the fluid domain, but not for the solid domain in these simulations. Moreover, for solids, $u_i = 0$.

2.2.2. Geometry, mesh generation and boundary conditions

The CFD simulations for this part of the thesis were carried out for 2 different geometries: A simplified geometry and a full generator model. The latter based on the geometry previously used by Jamshidi (2017).

The simplified geometry for the simulations is based on the electric generator described by Wallin et al. (2010) and Figure 10 to the left shows a simplified schematic of a sector in angular

direction for that generator. Only a ventilation channel is used for the simulation and the dimensions are based on the description by Wallin et al. The space between the stator winding and the spacers have been defined as downstream (DS) and upstream (US) ducts for ventilation, which are on each side of the coil. The right image in Figure 11 shows the front of the computational domain as seen from the air gap (representing a ventilation channel). The figure also shows how some of the boundaries are defined and some of the regions conforming the domain. The computational domain consists of a fluid region (Air) and 4 different solid regions (Insulation, Coil, Spacers and Stator Core) with a special boundary condition for the coupling among the different regions. The materials are defined for the different regions and three different volumetric heat sources were used between 3×10^5 and 1.2×10^6 W/m^3 for the coil and 2×10^4 and 8.2×10^4 W/m^3 for the stator core. The velocity boundary condition for the air at the inlet was a fixed velocity with averaged tangential, radial and axial components, taken from the results of the flow field obtained by Jamshidi (2017), giving a range of Re_{DH} based on the hydraulic diameter of the DS within the range 3000-17000.

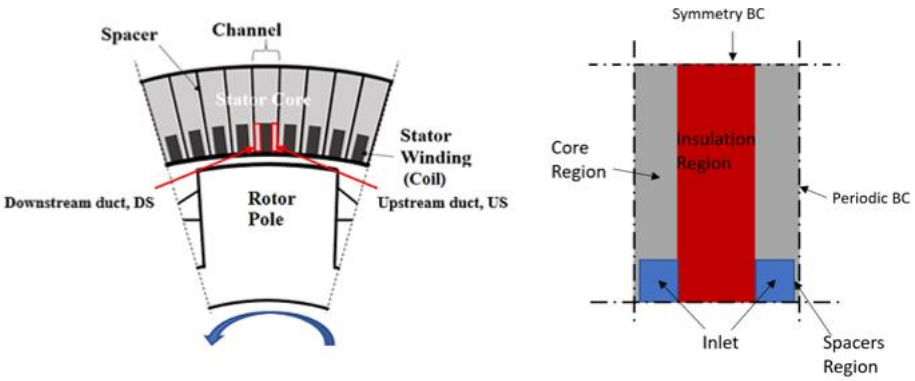

Figure 11. Schematic cross-section of generator with some parts (left) and some definitions of boundaries and regions (right). In the right figure, the blue coloured region represents air, grey region represents stator core and spacers while red region represents the coil with insulation.

The geometry of the stator generator model was taken from the one used by Jamshidi (2017), and in Figure 12 the complete domain used by Jamshidi (2017), the mesh and the part of the domain that is used for this part of the thesis (enclosed by dashed lines) are shown. The computations were done in a domain consisting of a block-structured mesh with total number of cells of 4.1M and the wall y^+ value was kept lower than one. The domain that was used in the present part of the study consists of the stator channels and the outlet and the idea behind using a part of the complete domain is to save computational time. The same nomenclature for

the ducts at each side of the coils is kept (DS and US). A "pick-up", which is described in detail by Jamshidi (2017) was also kept for the spacers. Three different cases with different Re_{DH} were simulated using this domain. The inlet boundary condition of one of the cases was a non-uniform velocity distribution with tangential, radial and axial components, obtained from the results of one of the cases reported by Jamshidi (2017) with a mass flow rate of 0.16 m^3/s. The inlet boundary condition for the other three cases resulted from scaling the velocity. Other boundary conditions, no-slip condition for the walls, cyclic boundary conditions at each side of the computational domain, the walls of each ventilation channel were set to be isothermal with a prescribed value of the temperature and the heat flux.

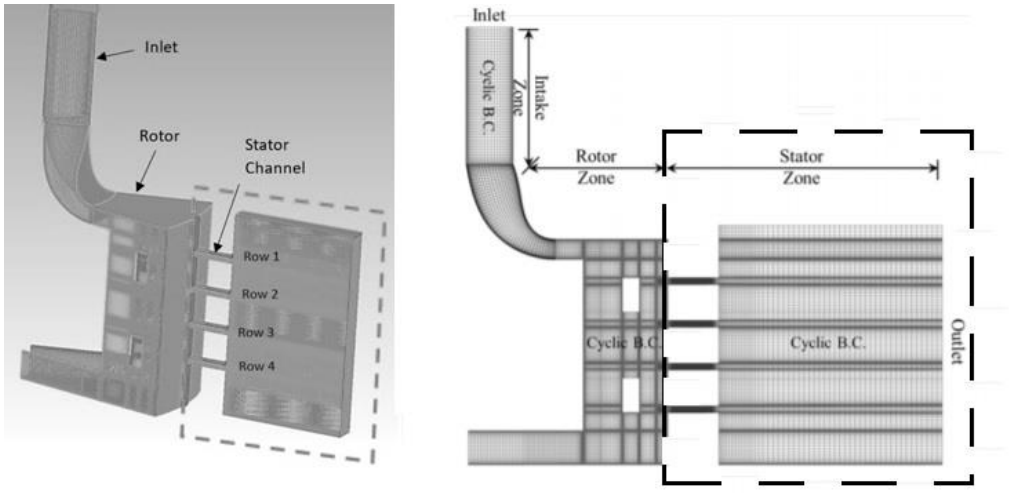

Figure 12. Computational domain of current study as a part of the domain used by Jamshidi (2017). Domain of current study is enclosed by the dashed lines and includes the stator and outlet of the domain used by Jamshidi (2017).

For both the simplified and generator model geometries, the meshes were obtained in ICEM CFD. For the simplified geometry, a mesh sensitivity study and discretization error study were performed.

2.2.3. Numerical aspects

Simulations using the simplified geometry and the stator generator model were carried out with the shear stress transport (SST) $k-\omega$ turbulence model. The Limited Linear numerical scheme was used for discretizing the momentum equations. This is a second-order scheme that limits towards first order in regions of rapidly changing gradient (OpenFOAM User Guide, 2018).

Convergence is reached with at least three orders of magnitude decrease in the residuals for the solved momentum and energy equations.

2.3. Discretization errors in CFD simulations

A discretization error analysis of the meshes has been carried out for two of the domains used in this thesis. These meshes correspond to the flow over arbitrary rough surfaces and the study of the heat transfer using a simplified geometry of the stator channel in an electric generator. This discretization analysis is carried out following the GCI method described by Celik et al. (2008). At least three different mesh resolutions should be used in order to evaluate a key variable, β, according to the solutions given by each mesh resolution. For the rough surface simulations, the key variable to be evaluated was the wall shear stress and for the heat transfer studies, the Nusselt number. The initial spacing in the mesh is determined from which the mesh refinement factors (r_{21}, r_{32}) are obtained. For this study, the refinement factors were not the same. The apparent order of accuracy, p, is then calculated from

$$p = \frac{1}{\ln(r_{32})}\left|\ln\left|\frac{\varphi_{32}}{\varphi_{21}}\right| + q(p)\right| \tag{25}$$

$$q(p) = ln\left(\frac{{r_{21}}^{p} - s}{{r_{32}}^{p} - s}\right) \tag{26}$$

$$s = 1\ sgn\left(\frac{e_{32}}{e_{21}}\right) \tag{27}$$

where $\varphi_{32} = \beta_3 - \beta_2$, $\varphi_{21} = \beta_2 - \beta_1$ and $q(p)$=0 if r_{21}= r_{32}. The relative errors are estimated by

$$e_{32}=\left|\frac{\beta_2-\beta_3}{\beta_2}\right|. \tag{28}$$

If the coarse grid solution is considered, the grid convergence index, GCI, is calculated as

$$GCI_{coarse}^{32}=\frac{1.25e_{32}\,r_{32}^{p}}{r_{32}^{p}-1}. \tag{29}$$

The value that is obtained as GCI is analogous to experimental uncertainties and indicates the range in which the actual value of the β is expected to fall.

2.4. Limitations of the CFD simulations

Many variants from the defaults $k-\varepsilon$ and $k-\omega$ turbulence models have been proposed and tested, since there is a variety of situations and flows that cannot be modelled by a single turbulence model. Part of the complexity of the flow modeling resides in the proper prediction of separation, reattachment and recirculation, which are features that are present in the flows that were simulated in this thesis. Therefore, for each specific case, the selection of the right turbulence model might require some iterations by testing the different models. However, there is a lot of literature in turbulence modeling and example cases to help narrowing the choice of the best model for each particular case. Furthermore, the accuracy of the prediction can be increased if care is taken in selecting the numerical scheme and discretization that work best for that application. Therefore, the modeling of flows presented in this thesis can be improved substantially when all these factors are assessed properly. For heat transfer this is very important because the transfer of heat is affected by separation, recirculation and reattachment. Also, for cases of conjugate heat transfer, it is important to remember that heat is transferred from a solid to a fluid by conduction at molecular level and therefore, refined meshes in this fluid-solid interface are required to model this transference and the large temperature gradients present across the boundary layers.

Regarding the resolved simulation of rough walls, the same factors have to be considered before a definitive model is established. However, a problem resides in the fact that not all the surfaces can be described with the same roughness functions and therefore, finding a turbulence model that could be used for simulating flows over any surface can be challenging. The indirect prediction of the roughness function relies on the accurate prediction of the wall shear stress, which is importantly affected by separation and therefore, this could be the main criteria for selecting the turbulence model and numerical schemes to be used in the future. The prediction of turbulence at low Reynolds numbers is also another factor to consider when choosing the right model, since overprediction of the wall shear stress was observed for some simulations of roughness in this thesis.

It is clear that more accurate results can be obtained if different modeling approaches are used i.e. LES and/or DNS. However, the cost of using these modeling approaches are still prohibitive in most cases. RANS, on the other hand, is much cheaper in terms of resources and more available alternative to be used by engineers.

3. Experiments

This chapter will describe the experimental setup that has been followed to carry out the work that is presented in this thesis. The methodology is discussed separately for both engineering applications.

3.1. Friction Drag of Rough Surfaces

A rotating disk rig was designed and constructed for micro-PIV and torque measurements. The disk is driven by an electric motor and rotates inside a 20-liter tank filled with water at around 20°C. A schematic of the rig is shown in Figure 13.

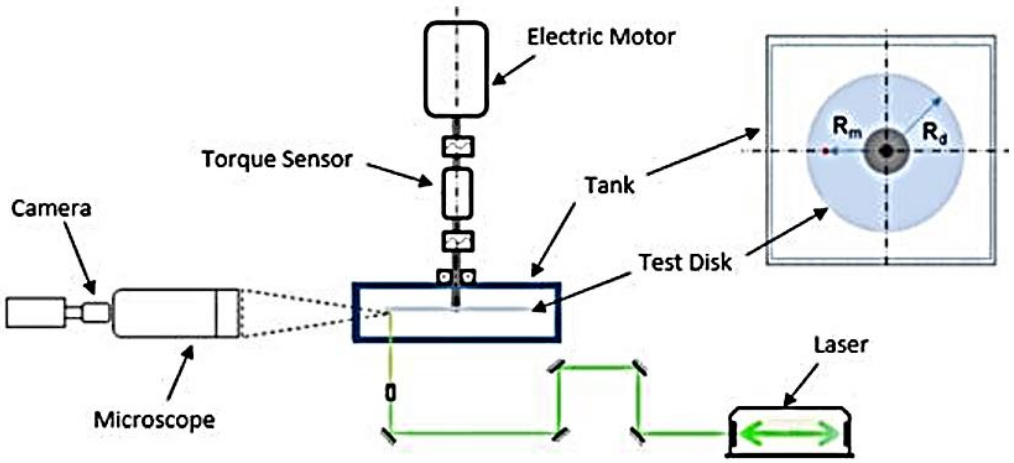

Figure 13. Schematic of the rotating disk rig

Different disks with different roughness were used for the experiments. These include one smooth disk for reference, two cases with sandpaper, three cases of disks with different antifouling painting applications (corresponding to roughness A, B and C explained in section 3.1) and one case with periodic roughness was also used. Table 1 illustrates the different cases and their average roughness. For the periodic roughness, the peak value of roughness is given.

Table 1. Average roughness height for the experimental cases

Smooth	A	B	C	80-G	400-G	Periodic
0.55	13	33	55	201	35	500

3.1.1. MicroPIV Measurements in Rough-Wall Boundary Layers

Measurement of boundary layer profiles on disks is a challenging task due to very small thickness of the boundary layer (3 – 5 mm). In order to measure the azimuthal velocity component near the disk wall with the high spatial resolution and to capture the inner layer of the turbulent boundary layer, a microscopic optics was used with magnification 12 times.

The seeding of the flow was done by using PMMA particles from Microparticles GmbH with 1 μm in diameter. The images were registered, magnified and transferred by a monochrome double-frame CCD camera with resolution 2048 × 2048 pixels^2, 14-bit pixel depth and 7.4 μm pixel size. The recording of this camera was synchronized with the specific angle of rotation of the test disk through a hall sensor. The registered images had particle images in the form of a diffraction pattern with a central circular part and several rings around it as shown in Figure 14 (left). It was important to locate the wall in the images and therefore, a 10 mm radial insert made of PMMA plastic was embedded as shown in Figure 14 (right) to provide a reflective surface. The wall position was calculated as a line going through the middle point of a line segment that connects particles and their reflections from the top and the bottom of a recorded image. Another reason was to reduce the light scattering caused by the rough surfaces and reduce the noise. The data was processed by identifying particles in every pair of images by means of a particle image tracking method with the help of a correlation of particles in every image by the Airy diffraction disc template intensity distribution.

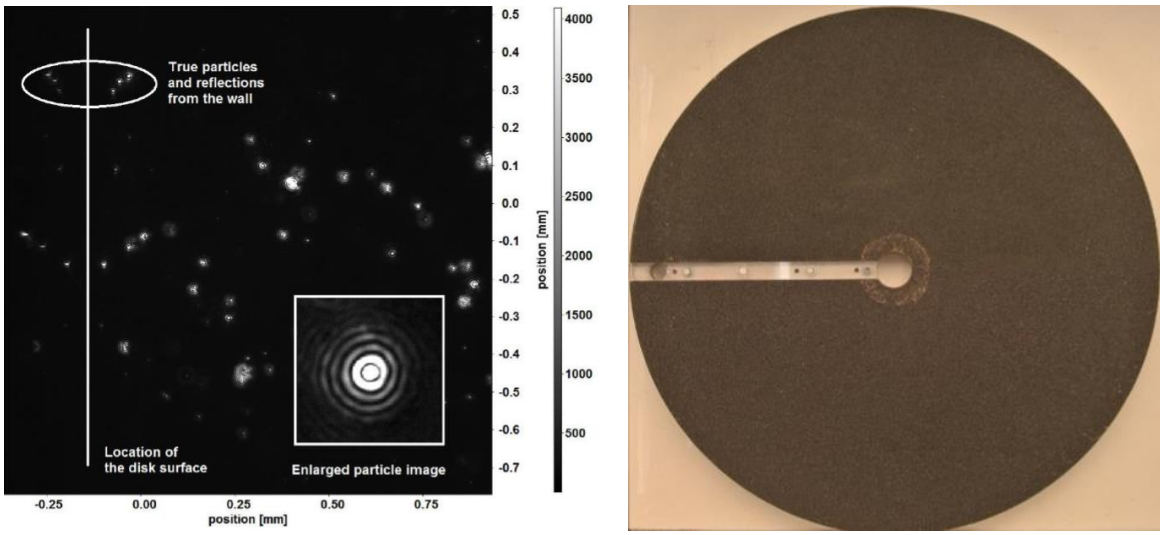

Figure 14. Left: Example of particle images and their reflections by the wall. Right: Rough disk with the PMMA insert installed.

For the geometrical calibration of the measurement field, a wire with a known diameter of 0.85 mm was imaged in the measurement area before the actual experiment. The diameter of the wire was measured on the recorded image. Using the obtained calibration and the frame separation time, the displacement of the particle was converted into velocity data. The accuracy of finding the wire edges was estimated to be 5 px and the wire image was 400 px, which yield an estimation of the accuracy of the calibration to be ~3%.

The accuracy of the particle identification algorithm could be assessed as 0.5 px due to the relatively large particle diameter 8 px. Hence, for two identifications of start and end positions, the accuracy of the obtained particle displacement is around 1 px which is equal to ±0.36 m/s for the disk rotational speeds of 300 and 600 rpm. The assessment of the accuracy of the obtained mean velocity profile gives 0.5% of error.

Another source of potential error is the perspective projection of particles on the recording plane. The main assumption here is that the particle is moving in a plane that is parallel to the recording plane. During the experiments, the recording camera has been located and positioned in such a way that the plane of the recorded image is parallel to the direction of the tangential component of the velocity of the fluid. Since the dominant velocity component in a rotating disk is the tangential velocity, then radial components of velocity are not expected to occur and influence the results, since the particle is always moving in a tangential plane. The PIV measurements rely on the performance of different equipment (microscope, camera, laser, etc.)

and therefore, the sources of errors due to a bad usage or deficient performance of the different equipment increase.

Another important aspect is the seeding of particles. If the seeding is scarce, the error increases because more particle image pairs increase the strength of the statistical analysis. On the other hand, excessively seeded flows can modify the viscosity of the fluid. It has been determined by experience that 10 particles of 1 μm diameter in an interrogation volume of 25^3 μm^3 is a good measure.

The results of the measurements are presented as velocity profiles U^+vs y^+, both depending on the value of the wall shear stress. The Clauser method (Clauser, 1956) of assessment of the shear stress for the smooth disk can be used, since the free stream velocity (tangential component of the velocity of the disk at the edge) is known and the different velocities from the wall can also be determined from the PIV measurements. The Clauser method expresses the log-wall in terms of the free stream velocity and the friction velocity, which would be the only unknown term that needs to be determined, assuming κ and the log-wall constant B to be 0.41 and 5. Therefore, the wall shear stress is varied until the resulting line lies on the log-law region of a turbulent boundary layer. If this is done for a wide range of Reynolds numbers, then a correlation that relates skin friction coefficient and Reynolds numbers can be obtained. For this thesis, the correlation that was obtained is shown in Figure 15. The relative error due to the scattering of the experimental data, from which the fitting curve can be obtained was 1.9% for the skin friction coefficient. If the skin friction is known for smooth surfaces, then for rough surfaces can be determined because the torque can be expressed as a function of the skin friction coefficient, the radius of the disk and the angular velocity, $T=f(c_f, \omega, r)$. Thus, for a rough disk with same radius and angular velocity, the difference in torque is only a consequence of the increment in the skin friction coefficient. It is then possible to infer that the accurate determination of the wall shear stress for the rough disk depends on how accurate the determination of the skin friction coefficient for the smooth case is.

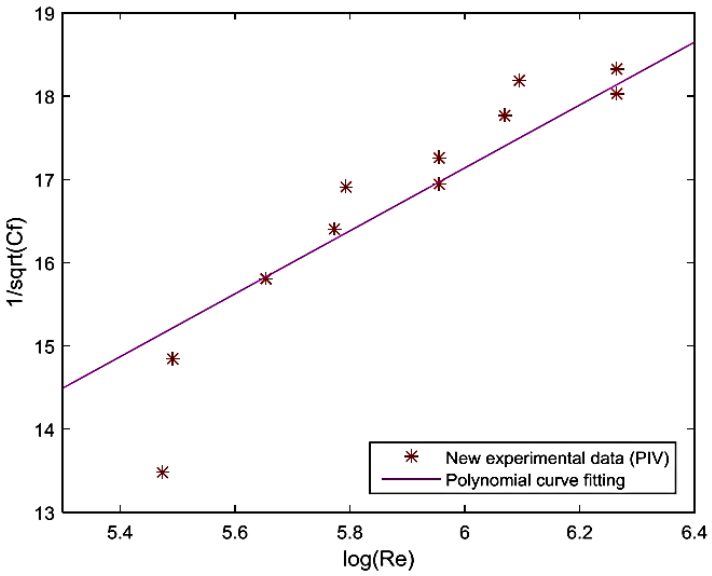

Figure 15. Dependence of the skin friction coefficient and Reynolds number from PIV experimental data.

3.1.2. Torque Measurement Tests

For the torque measurement test, a Kistler type 4503A torque meter was installed on the rotating disk rig connecting the electric motor and rotating disk shaft (as shown in Figure 13). The torque sensor operates based on the strain gauge principle. The torque meter output was monitored by an analogue to digital converter (ADC) controlled by a PC. The torque was measured for rotational velocities from 0 to 1200 rpm. The measurement procedure has included a warm-up of the running rig and the measurement equipment for at least one hour before experiments. Disks coated with antifouling paints with different roughness were used for the tests and a smooth disk for reference.

The measurements of the torque include a first measurement of the torque without disks, because the shaft, bearings and other mechanical couplings are contributing to the total torque. This torque without disks should be subtracted to the torque measurements with disk to obtain the net torque contribution by the disks, which is the parameter of interest.

It is important to avoid bubbles as much as could be possible. The bubbles in the water will gather close to the disk surface and can potentially influence the torque measurements. The disk consists of two surfaces and its edge. In torque measurements with rotating disks, what is of interest is the torque that is caused by the surface of the disk. Since the edge of the disk also

contributes to the torque, then this contribution should be determined and subtracted from the total torque. This can be done by running torque measurements with disks of different thickness. If it is assumed that the surface finish is the same for all the smooth disks, then the increment or the difference in torque will be caused by the difference in the thickness of the disks.

The accuracy and repeatability of the measurement is given as 0.01 Nm and the standard error was determined by repeating the procedure of measuring the torque for different radial speeds in ascending order and then in reversed order. Another source of error that is worth of mentioning is the presence of a rubber seal mounted to prevent leakages of water from the tank on the shaft side. The friction between this seal and the shaft is sensitive to changes in temperature and therefore, to minimize this effect, a warm-up of the seal (by running the facility without measuring) is recommended and was done before any measurement.

Finally, the mounting of the different elements is also important to avoid influence on the measurements. The main shaft was carefully aligned with the torquemeter shaft and the electric motor shaft.

3.1.3. Towing Tank Tests

Towing tank tests were performed by the Norwegian Marine Technology Research Institute (MARINTEK) and reported by Savio et al. (2015). In summary, test plates with different roughness A, B and C (previously mentioned in section 2) were towed in the wake of a leading (front) plate which was smooth. The Reynolds number during tests was based on the total length of plates and ranged between 3×10^7 and 9×10^7.

3.2. Hydropower electric generator

Figure 16 shows the rig used for the electric generator experiments. This rig consists of a hydro-generator model with an inlet section, a rotor coupled to an electric motor, a stator and a fan to supply air flow at a rate of 0.16 m^3/s with the aid of an external fan. The rotor and stator are manufactured by rapid prototyping. The rotor has 12 poles and rotates in the counter-clockwise direction, looking from above, at 2000 rpm. The stator has 4 rows of ventilation channels along the rotation axis and 108 ventilation channels per row, separated by spacers.

One sector of the original stator consists of removable transparent pieces for optical access to the interior of the generator, as shown in Figure 16. The removable sector corresponds to 4 ventilation channels in the angular direction, and there is one piece for each channel row.

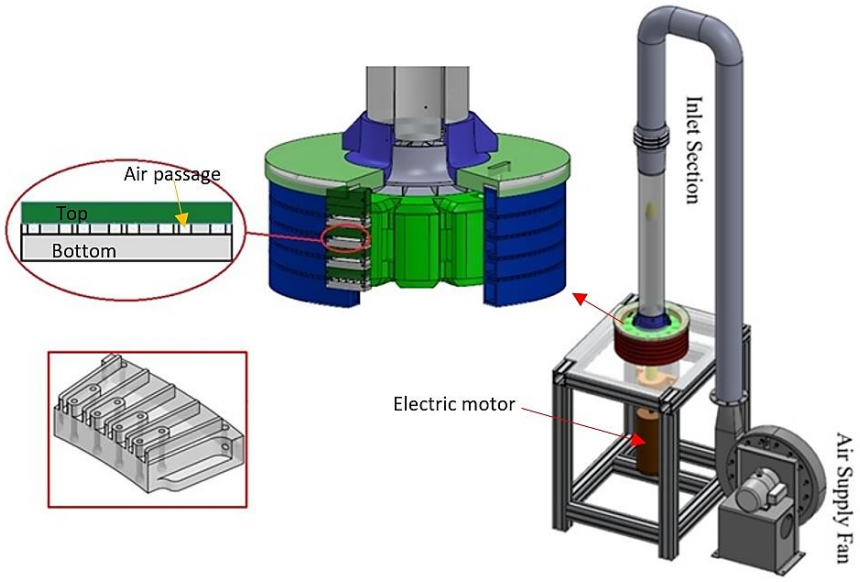

Figure 16. Schematic of the electric generator rig.

3.2.1. Naphthalene Sublimation Technique

The naphthalene sublimation technique was used for studying the convective heat transfer occurring in the ventilation channels and therefore, the stator walls should be made of naphthalene, but only the top removable flat piece was made of naphthalene, thus limiting the study to that surface of the ventilation channels (see an oval insert in Figure 16). A mold was therefore manufactured using rapid prototyping leaving some volumes that will be filled with naphthalene. The naphthalene is filled only between parts looking like the coils and spacers, corresponding to the surfaces that are in contact with the air. The result is a flat surface with naphthalene, as seen at the left image in Figure 17.

The naphthalene sublimation rate is in this case evaluated in two different ways, by weighting and scanning. The scanning involves an intermediate step where imprints of the specimen are taken using a dentistry elastomeric impression silicone and these imprints are taken from all the specimens before and after the tests. Internal features of the mold are defined as references to be located with high accuracy before and after the tests, to be used to align the data during analysis. The right image in Figure 17 shows one of the imprints. A laser scanner MikroCAD

Lite with measurement area 26×20 mm^2 is used to measure the shape of the imprints in 3 areas for each ventilation channel imprinted. The bulk sublimation rate is also measured by weighting the specimen before and after the experiments with a scale that has a resolution of 10 μg, operating at an average temperature of 27±1°C.

The prepared naphthalene specimen is then mounted into the generator model once imprints are taken and the specimen is weighted. The external flow fan and rotor rotation motor are then switched on. After 25 minutes of operation, the facility operation is stopped, the naphthalene specimen removed, imprints and weights taken.

Figure 17. Left: Resulting naphthalene specimen. Right: Imprint taken from a specimen and the 3 areas of interest for scanning.

4. Summary of the papers

This chapter gives a short summary of the main contents and results reported in the appended papers.

4.1. Paper I

B. Niebles Atencio, M. Tokarev and V. Chernoray (2016) "Submicron Resolution Long-Distance Micro-PIV Measurements in a Rough-Wall Boundary Layer", 18th International Symposium on the Application of Laser and Imaging Techniques to Fluid Mechanics, Lisbon.

4.1.1. Division of work

Niebles Atencio participated in building the tank for the rig, performed the experiments together with Tokarev, participated in the post-processing of the experimental results, performed CFD simulations with their post-processing and carried out the analysis of the results and writing of the paper. Tokarev prepared set-up of the experimental equipment, performed the experiments with Niebles Atencio, took care of the post-processing and provided feedback on the analysis of results and writing. Chernoray supervised the planning, the rig design and manufacturing, the set-up of the experiments and provided feedback on the analysis of results and writing.

4.1.2. Summary and discussion

This paper shows a method for obtaining the roughness function of different surface roughness by using a small-scale rig with rotating disk and a long-distance microscopic PIV in order to obtain submicron resolution inside the boundary layer that is developed on the disk during rotation. The measurements were performed on disks with different degree of roughness and these are a smooth disk, three antifouling coatings used in marine applications, two cases of sandpaper roughness and a periodic roughness. The rotational speeds were 300 rpm and 600 rpm. Every point of the mean velocity profile was based on nearly 200 instant velocity values that were obtained from 2000 PIV image pairs by using particle tracking approach. The results of the wall shear stress study of the smooth disk were used together with the results from torque measurements and from the micro-PIV results to get the dimensionless velocity profiles. From the dimensionless velocity profiles the roughness function was obtained and compared with the

roughness function obtained from the resulting velocity profiles of the CFD simulations and the roughness function from an equation derived by Hama (1954). The resulting velocity profiles from the experiments, as expected, are shifted downwards due to the presence of the roughness as shown in Figure 18 for one of the rough antifouling coatings. The agreement of the experimental results with CFD simulations (similar velocity profiles) is better for low roughness values. It was found that CFD simulations of arbitrary roughness is quite challenging and requires a very good mesh in order to resolve the boundary layer. The experiments show that the smooth velocity profiles from micro-PIV agree perfectly with the smooth theoretical velocity profile and for the cases with roughness, the downshift is present in the velocity profiles, but more studies and validations are required. Micro-PIV can be useful not only for understanding how the roughness affects the velocity profiles and contributes to the drag, but also to provide more insights into the turbulence inside the boundary layer.

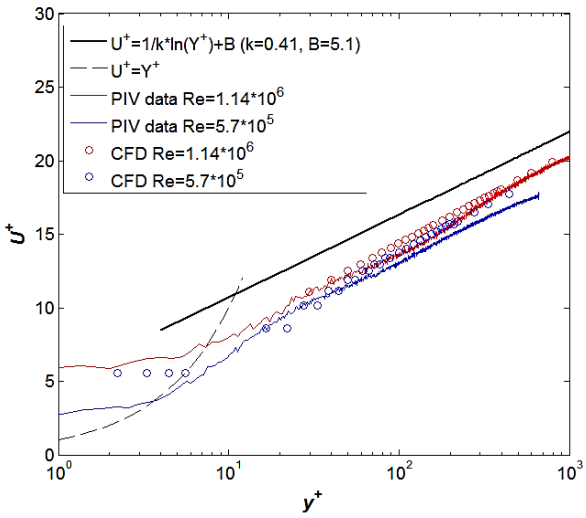

Figure 18. Dimensionless velocity profile from PIV results and CFD for one of the antifouling paints.

4.2. Paper II

B. Niebles Atencio, V. Chernoray (2017) "A Resolved RANS CFD Approach for Drag Characterization of Antifouling Paints". Ocean Engineering. In Press.

4.2.1. Division of work

Niebles Atencio participated in the design of the rig tank, setup of the experiments with the rotating disks, performed the experiments together with Chernoray, performed CFD simulations

and the post-processing of the CFD results, participated in the post-processing of the rotating disk and flat plate results, performed the analysis of the results and wrote the paper. Chernoray supervised the planning, the rig design and manufacture, performed experiments with Niebles Atencio, participated in the post-processing of the rotating disk and flat plate results and provided feedback on the writing of the paper.

4.2.2. Summary and discussion

This paper shows a method for obtaining the roughness function of any arbitrary rough surface by using resolved RANS simulations in channel flows. The idea is to provide a cheaper method in terms of resources and time when compared with experiments and other modeling approaches such as LES and DNS. This study was performed for a particular antifouling paint with different roughness used in marine applications. Indirect methods for the characterization of the drag and the roughness function were used for Reynolds numbers based on channel height in the range of 84000 to 280000. The roughness functions from resolved RANS simulations were compared with roughness functions obtained for the same coating from two of the most commonly used experimental techniques: a rotating disk rig and a towing tank. The data obtained from all three methods were successfully fitted on the same roughness function curve, which is shown in Figure 19. The results show in general, that roughness function of this particular antifouling coating followed the Cebeci and Bradshaw (1977) curve, which is already used in CFD software to account for roughness and is based on the Nikuradse sandgrain roughness function curve. The roughness Reynolds number was based on the rms of the roughness height and it was found that this was a good roughness height parameter to collapse the data into the roughness function curve without the need of using texture parameters. The spread of the data from CFD simulations and two different experimental facilities in this study is reasonable. The determination of the roughness function via indirect methods is a very useful alternative when the velocity profiles are not available or of insufficient quality. It has been widely known and discussed by many researchers that the characterization and roughness function determination is individual and not general. Ideally, it would be good to have a large database of results from different surfaces and try to collapse all this data into a single curve using a proper scaling parameter, but this would require a lot of efforts and time. This is what makes the drag characterization of rough surfaces very challenging. From the other hand, the developed resolved CFD method could be a new alternative to characterize any particular

surface roughness and eliminate the need of universal correlations, but the accuracy of the CFD simulations should be increased and this is something that needs to be tackled in the future.

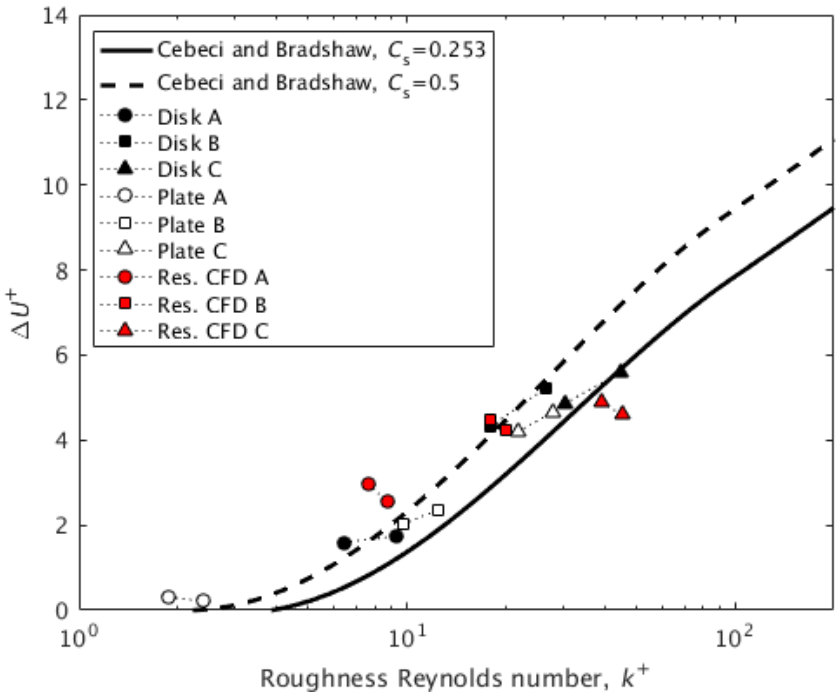

Figure 19. Comparison of roughness functions from experiments and resolved CFD.

4.3. Paper III

B. Niebles Atencio, H. Nilsson (2018) "Evaluation of convective heat transfer correlations for network modelling of electric generator stator channels, based on conjugate and convective heat transfer CFD simulations". Paper to be submitted for publication.

4.3.1. Division of work

Niebles Atencio created geometries for CFD simulations, performed a grid sensitivity analysis, determined the discretization error of the CFD simulations, performed the CFD simulations, post-processing, analysis of results and writing of the paper. Nilsson supervised the planning, the CFD simulations and gave feedback on the analysis of results and the writing.

4.3.2. Summary and discussion

In this paper, conjugate and convective heat transfer simulations were performed in order to determine a convective heat transfer correlation specifically for squared-shaped stator channel ducts of electric generators that can be used for their design. During the design stage of these machines, the convective heat transfer is commonly approximated using empirical correlations. These correlations were developed for a range of Reynolds numbers, geometries, and flow conditions that are not necessarily appropriate for electric generators and if the heat transfer is not accurately estimated, the cooling system will not perform at its best, leading to an increase of losses and reduction of the efficiency. Equation 30 is the resulting correlation from this study and was compared against empirical correlations found in the literature, but also with results from the convective heat transfer simulations in a more complete electric generator stator model. Results are depicted in Figure 20. It is shown that the commonly used correlations differ from the one obtained in the present study by around 20% over the entire range of Reynolds numbers. The results show that the heat transfer that is estimated using the correlation from this study is lower than the heat transfer that would be obtained from using the well-known and normally used experimental correlations.

$$\overline{Nu} = 0.0034 Re_{DH}^{0.9679}. \tag{30}$$

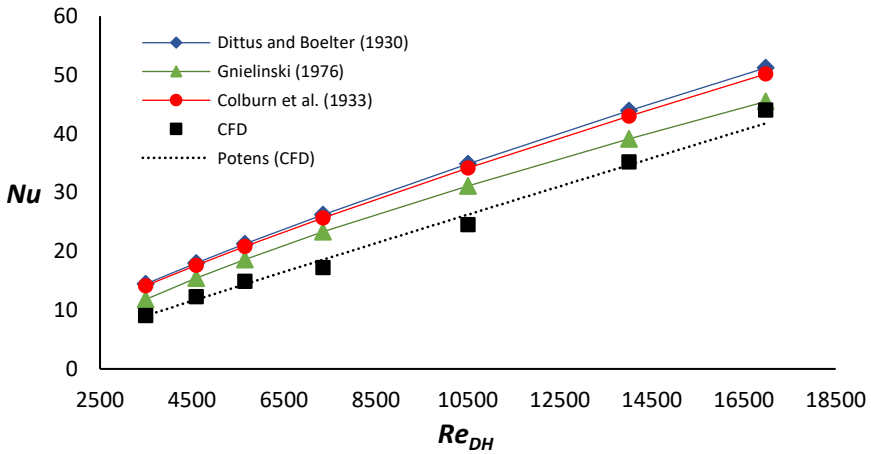

Figure 20. Variation of the Nusselt number with Reynolds number for a stator channel of electrical generator. Current CFD correlation is compared to some widely used experimental correlations.

The correlation that was determined from this study is used in the network model that was developed by Cabré Gimeno (2017). The Gnielinski correlation was also used in that network model. The purpose of this is to assess the performance of the heat transfer from using one of

the most well-known correlations compared to the performance of the heat transfer from the correlation determined in the present study. The resulting heat transfer and temperatures in the core, coil and the cooling air are shown and can be compared to those that would be obtained if the Gnielinksi correlation is used in the network model instead. See Table 2.

Table 2. Results from the network simulations using Eq 30 and a correlation from literature

	Present study				**Gnielinski**			
Re	4779	6372	9558	12744	4779	6372	9558	12744
Nu	12.4	16.3	24.2	32	15.1	19.3	26.8	33.6
$\mathbf{T_{coil}}$ **,°C**	69.5	66.1	61.9	59.3	69.5	65.9	61.7	59.2
$\mathbf{T_{core}}$ **,°C**	47.8	44.5	40.5	38.1	47.9	44.4	40.4	38.0
$\mathbf{T_{air}}$ **,°C**	61.9	50.6	39.8	34.6	62.0	50.6	39.5	34.5

Table 2 shows that the Gnielinski correlation predicts an average of around 14% higher heat transfer compared to the correlation derived from the present study and this is reflected in a generally lower temperature of the coil and stator core, when the Gnielinksi correlation is applied. The table shows that more cooling might be required when the experimental correlations are used in network simulations for the design of electrical generators.

4.4. Paper IV

B. Niebles Atencio, H. Jamshidi, M. Liljemark, H. Nilsson, V. Chernoray (2018) "Assessment of the Naphthalene Sublimation Technique for Determination of Convective Heat Transfer in Fundamental and Industrial Applications". Paper to be submitted for publication.

4.4.1. Division of work

Niebles Atencio created the naphthalene mold for the experiments in the generator model rig, performed the experiments and CFD simulations for the generator model case, participated in the scanning and scaling of the naphthalene specimens, important for the post-processing, post-processed and analyzed the results, and complemented an initial draft of the paper written by Jamshidi including the generator case model. Jamshidi designed the rig for the impinging jet

experiments, created the impinging jet case for CFD simulations, performed experiments for the impinging jet case, post-processed the results from CFD simulations and experiments of the impinging jet case, analyzed the results and wrote the impinging jet part of the paper. Liljemark measured the surface of the naphthalene specimen for the impinging jet case. Nilsson and Chernoray gave feedback in the writing of the paper.

4.4.2. Summary and discussion

The naphthalene sublimation technique was assessed as experimental method for indirectly determining the convective heat transfer for two cases: an impinging air jet on a flat surface and for the analysis of the heat transfer occurring in the stator core of an electric generator model. The turbulent impinging jet is fully developed due to a large length to diameter ratio of the circular straight nozzle. Two Reynolds numbers based on the nozzle exit condition, 15000 and 23000, and two nozzle diameter distances from the jet exit to the surface, 6 and 8, are considered. For the electric generator model, a fully turbulent internal flow with a Reynolds number of 4120 is considered, based on the hydraulic diameter of the stator ventilation ducts. The evaluation of the sublimation rate in the generator model case was done by two ways: scanning the sublimed surface before and after the experiments and by weighting the naphthalene specimen before and after the experiments. The process of creating the naphthalene specimen was found to be quite critical and important for the success of the experiments. The results of the impinging jet case were compared against former experiments carried out by different researchers and also compared with CFD simulations. The generator model experiments in this case were compared with convective heat transfer CFD simulations. The agreement between CFD and experiments is better for low Reynolds number in the impinging jet case and for the generator model, it is found that there is around 9% overall difference between experiments and CFD simulations for the different rows of the generator model. The heat transfer is lower in the first rows of the generator model and increases in subsequent rows (see Figure 21). The experimental heat transfer results depend on the way the sublimation rate is evaluated. The scanning is predicting systematically higher values of heat transfer than the weighting, but in overall the difference was not larger than 17%. This is the first study so far that provides a comparison of CFD simulations and experimental data from the naphthalene sublimation technique. The results showed that the naphthalene sublimation technique is a very good alternative for determining the heat transfer for both fundamental and industrial applications.

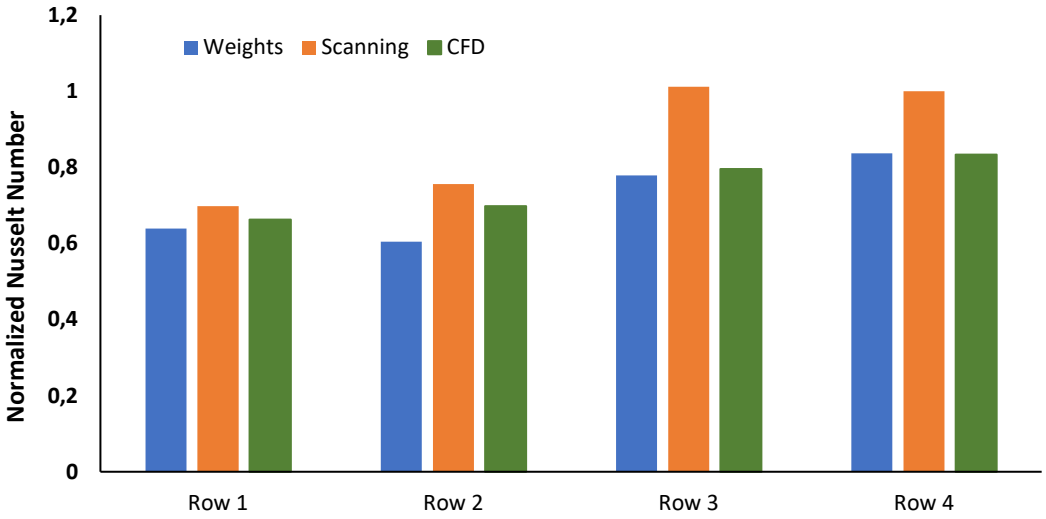

Figure 21. Comparison of the heat transfer in the stator channel of electrical generator from the CFD simulations and experiments.

5. Concluding remarks

This thesis treated two engineering applications separately. These applications are apparently not related, but they do share the need of being more efficient from the energy point of view. In the following, some concluding remarks can be drawn for the two treated applications in a separated way.

5.1. Friction Drag by Rough Surfaces

The micro-PIV experiments showed to be a new promising alternative for evaluating the roughness function for surfaces with any roughness type. The roughness function is evaluated using the roughness function definition, from velocity profiles that can be obtained after the post-processing of the experimental results. The drawback lies on the complexity involved in performing the experiments, the cost of acquiring the required equipment and the fact that the dependence on different equipment for the experiments increase the number of error sources. During the experiments, it was found that the boundary layer can be thoroughly inspected and therefore, micro-PIV could be useful for the experimental study of flow features in boundary layers for any case and application. Indirect methods for obtaining the roughness function could be also used with micro-PIV results by determining the wall shear stress using the Clauser method. Interesting results could be obtained if the determination of roughness functions via micro-PIV are compared with other experimental alternatives.

The main drawback of micro-PIV for the determination of roughness function is that it requires the knowledge of the wall shear stress to obtain scaled velocity profiles. Thus, the wall shear stress still needs to be measured somehow or to be determined with the Clauser method. In this work, torque data was used for measuring the wall shear stress. Therefore, PIV data was not used in the analysis of roughness function, but only torque data with the indirect method instead.

Torque measurements were found to be relatively easy to perform and useful for assessing drag with indirect methods using rotating disks. The post-processing is also not complicated. During this work, guidelines for measurements and post-processing were developed. This experimental technique is an excellent alternative for evaluating the roughness function for antifouling paints and any roughness with relatively low cost. The comparison with towing tank tests and CFD was satisfactory and is a technique that works well with micro-PIV.

The CFD-based approach that was proposed is useful because it can be a much less expensive alternative than experiments and other modeling approaches (LES/DNS) to find, with acceptable reliability, the roughness function of antifouling coatings and surfaces with arbitrary roughness. Once the roughness function has been determined for a particular surface, predictions of drag can be made for that surface. The procedure for the drag characterization of antifouling paints with CFD involves a proper scanning of the surface under study and therefore, it is critical to have a good and accurate scanning procedure.

The majority of the roughness function studies that can be found in the literature involve finding the velocity profiles to get the roughness function (especially for CFD studies), but indirect methods have also shown to be very useful and well-established methods. In this thesis, results showed that the antifouling coating can also follow the Cebeci and Bradshaw curve and that no texture parameter of the roughness is needed to be used for determining the roughness length scale. However, the generalization of the roughness functions is a complex task because any surface can exhibit any roughness function and antifouling coatings can exhibit significantly different texture characteristics. Therefore, any generalized model will most probably fail when applied to some novel coating with an unusual roughness texture. Thus, the resolved CFD approach that was presented in this thesis would be valuable because it relies on the actual surface geometry rather than on a limited number of texture parameters.

Since the resolved CFD approach presented in this thesis for the roughness function determination of arbitrary surfaces rely on the wall shear stress, then the focus is on improving the prediction of this parameter. The results presented in this study showed that the turbulence model that was used might be overpredicting the wall shear stress for some velocity cases. This should be checked more carefully and maybe by testing other turbulence models. For the future, it would be also beneficial to validate the CFD approach against equivalent channel flow measurements and therefore, a channel flow facility should be designed, built and validated.

5.2. Hydropower electric generators

There is always room for improvement in engineering. The determination of a correlation for the heat transfer in the stator channels of electric generators by CFD is an attempt of finding a more suitable tool for designing of these machines to increase their efficiency. So far, all the correlations that are used in electric generators have been determined experimentally and this

would be the first one to be determined from numerical simulations. The reproduction of realistic conditions in the simulations is thus, critical for the success of this study. It would be desirable to have more correlations and in general, better tools for the design of more efficient machines.

It was found that the correlations normally used for predicting the heat transfer in the stator channels of electric generators might differ up to 20% with the results given by the correlation that was obtained from this study. The existing correlations were always giving higher values of the heat transfer. The problem of using correlations that give higher values of the heat transfer is that the cooling system is designed based on the estimated heat transfer. Therefore, the risk of designing a cooling system with lower cooling capacity than what is actually required is higher. This, in turn, potentially increases the risks of hot spots, lower efficiency and potential failure in the components of the electric generator.

For future work, more realistic geometries and CFD domains should be used. The influence of the turbulence model in the heat transfer should also be evaluated, and correlations for the accurate estimation of the heat transfer in other parts of the electric generator (such as the rotor-stator air gap) should be also attempted. Furthermore, the determination of correlations from experiments in a generator model rig would also be something to be considered in the future. Therefore, the development of new experimental techniques is a pertinent matter.

The naphthalene sublimation technique was found in this thesis to be an alternative for evaluating the heat transfer for fundamental and industrial applications such as hydropower electric generators. A critical step to get good quality naphthalene specimens is the procedure that is followed for creating the mold and for the molding of the naphthalene with the desired shape.

It is also important how the sublimation rate is evaluated (i.e., by naphthalene specimen weighting or by naphthalene surface scanning), since there are differences in the final results when using one or another evaluation method. It has been found that the weighting is very straightforward, but the accuracy of the scale should be high in order to avoid misleading results. If the desired method is the scanning of the naphthalene surface, then the use of imprints of the naphthalene surface is advisable to avoid the direct scanning of the naphthalene specimens, which in some cases can be disturbing due to the strong and characteristic smell of the naphthalene.

Future work with this experimental technique can be focused on trying to create naphthalene specimens for all the walls of the stator channels, so the heat transfer can be determined for different Reynolds numbers and thus, corroborating the CFD simulations for the development of correlations in electric generators. Correlations for the cooling of the rotor and the rotor-stator air gap are also required and could also be attempted with this technique.

Another study to consider is the use of some heat transfer enhancement features in generator channels (riblets, for instance). This can be investigated with naphthalene sublimation technique and CFD simulations. However, it should be analysed how feasible is to implement such features in the stator core of real generators in order to motivate this study.

References

Allen J J, Shockling M A, Kunkel G J and Smits A J. (2007). Turbulent flow in smooth and rough pipes. Phil. Trans. R. Soc A 365, pp. 699–714.

Ashrafian A, Andersson H and Manhart M. (2004). DNS of turbulent flow in a rod-roughened channel. Int. J. Heat Fluid Flow 25, 373–383.

Bhaganagar K, Kim J and Coleman G. (2004). Effect of Roughness on Wall-Bounded Turbulence. Flow, Turbulence and Combustion 72: 463–492.

Bin X, GuoBiao G, Lin R, ZhenGuo L, DePing Fu, Rui C, ShuQin G, JinShui G. (2014). Studies on the structure of radial ventilation channel to improve the cooling capacity of large turbo generator stator. 17th Int Conference in Elect Machines and Systems (ICEMS).

Boglietti A, Cavagnino A, Staton D, Shanel M, Mueller Markus and Mejuto C. (2009). Evolution and modern approaches for thermal analysis of electrical machines. IEEE Trans on Industrial Electronics. 56 (3), pp. 871-882.

Boussinesq J. (1877). Essai sur la théorie des eaux courantes, Mémoires présentés par divers savants à l'Académie des Sciences 23 (1): 1-680.

Bumby J R and Martin R. (2005). Axial-flux permanent-magnet air-cored generator for small-scale wind turbines. IEE Proceedings-Elect Power Applications 152(5), pp. 1065-1075.

Cabré Gimeno M. (2017). Network modelling of cooling of hydro-generators. Master thesis, Chalmers University of Technology, Sweden.

Candries M and Atlar M . (2003). Estimating the impact of new generation antifoulings on ship performance: the presence of slime. J. of Marine Eng. and Technology 2, 13–22.

CD-ADAPCO, 2016. User Guide STAR-CCM+. Version 7.02.011.

Cebeci T and Bradshaw P. (1977). Momentum Transfer in Boundary Layers, Hemisphere Publishing/McGraw-Hill, pp. 176–180.

Celik I, Ghia U, Roache P, Freitas C, Coleman H, Raad P. (2008). Procedure for Estimation and Reporting of Uncertainty Due to Discretization in CFD Applications. J. of Fluids Engineering Trans. ASME 130, 078001-1-4.

Clauser F H. (1954). Turbulent Boundary Layers in Adverse Pressure Gradients, J. Aerosol Sci. 21, 91–108.

Clauser, F.H (1956). The Turbulent Boundary Layer. Adv in Appl Mechanics 4, pp. 1–51.

Colebrook, C. F, White, C. M. (1937). Experiments with Fluid Friction in Roughened Pipes. Proceedings of the Royal Society of London. Series A, Mathematical and Physical Sciences. 161 (906), pp. 367–381.

Colebrook C F. (1939). Turbulent flow in pipes, with particular reference to the transitional region between smooth and rough wall laws, J. Inst. Civ. Eng., 3, pp. 133–156.

Daily J. W. and Nece R. E. (1960). Chamber dimension effects on induced flow and frictional resistance of enclosed rotating disks. ASME Journal of Basic Eng. 82, Transactions ASME, pp. 217–232.

Demirel Y.K., Khorasanchi M., Turan O., Incecik A., Schultz M. (2014). A CFD model for the frictional resistance prediction of antifouling coatings. Ocean Engineering 89, pp. 21–31.

Ferziger J.H, Peric M. (2002). Computational Methods for Fluid Dynamics. Springer, 3th Edition.

Flack K A, Schultz M P and Shapiro T A. (2005). Experimental support for Townsend's Reynolds number similarity hypothesis on rough walls. Phys. Fluids 17, 035102.

Flack K. A. and Schultz M.P. (2010). Review of hydraulic roughness scales in the fully rough regime J. Fluids Eng. 132 paper 041203, pp. 1–10.

Granville P.S. (1972). The torque and turbulent boundary layer of rotating disks with smooth and rough surfaces, and in drag-reducing polymer solutions. Report 3711 Dept. of the Navy Naval Ship Res. And Dev. Center.

Granville P.S. (1982). Drag-characterization method for arbitrarily rough surfaces by means of rotating disks. J. Fluids Eng. 104, pp. 373–377.

Granville P.S. (1987). Three indirect methods for the drag characterization of arbitrarily rough surfaces on flat plates. J. Ship Research. 31, pp. 70–77.

Grigson C.W.B. (1992). Drag losses of new ships caused by hull finish. J. Ship Res. 36, pp. 182–196.

Dittus F W and Boelter L M K. (1930). Heat transfer in automobile radiators of the tubular type. University of California Publications in Engineering 2 (13), pp. 443-461.

Di Pasquale D and Rona A. (2009). A selective review of CFD transition models. 39th AIAA Fluid Dynamics Conference, San Antonio, Texas.

Fujita M, Kabata Y, Tokumasu T, Kakiuchi M, Shiomi H and Nagano S. (2005). Air-cooled large turbine generator with multiple-pitched ventilation ducts. IEEE International Conference on Electric Machines and Drives.

Gnielinksi V. (1976). New equations for heat and mass transfer in turbulent pipe and channel flow, Int. Chemical Engineering 16, pp. 359-368.

Hama F R. (1954), Boundary-layer characteristics for smooth and rough surfaces, Transactions of Society of Naval Architects & Marine Engineers, Vol. 62, pp. 333-358.

Hodgins N, Keysan O, McDonald A S and Mueller M A. (2012). Design and testing of a linear generator for Wave-Energy applications. IEEE Trans. on Industry Applications 47(4), pp.1716-1723.

Karlsson R.I. (1978). The Effect of Irregular Surface Roughness on the Frictional Resistance of Ships, In Proc. Int. Symp. Ship Viscous Resistance, L. Larsson, Ed., Swedish State Shipbuilding Experimental Tank, Göteborg.

Krogstad P A and Efros V. (2012). About turbulence statistics in the outer part of a boundary layer developing over 2D surface roughness. Phys. Fluids 24, 075112.

Incropera F, Dewitt D, Bergman T and Lavine A. (2013). Principles of heat and mass transfer, 7th Edition, Ed. John Wiley.

ITTC (1978). Performance Prediction Method. International Towing Tank Conference, 1978.

ITTC (2005). Report of the powering performance committee. International Towing Tank Conference, 2005.

Jamshidi H, Nilsson H and Chernoray V. (2014). Experimental and numerical investigation of hydro power generator ventilation. 27th IAHR Symp on Hydraulic Mach and Systems.

Jamshidi H, Nilsson H and Chernoray V. (2017). The effect of inlet flow rate on the air distribution in ventilation channels of a hydro-generator model.

Jamshidi H. (2017). Ventilation flow field characteristics of a hydro-generator model. An experimental and numerical study. PhD thesis, Chalmers University of Technology, Sweden.

Jimenez, J. 2004. Turbulent flows over rough walls. Ann. Rev. Fluid Mech. 36, 173–196.

Jo Daeseong, Al-Yahaia O, Altamimi Raga'I, Park J and Chae H. (2014). Experimental investigation of convective heat transfer in a narrow rectangular channel for upward and downward flows. J of Nuclear Engineering and Technology, 46 (2), pp. 195-206.

Klomberg S, Farnleitner E, Kastner G and Bíró O. (2015). Determination of the convective heat transfer coefficient in large electrical machines by a new simulation strategy. COMPEL: The International Journal for Computation and Mathematics in Electrical and Electronic Engineering, 34 (4), pp. 1335-1348.

Kunkel G and Marusic I. (2006). Study of the near-wall turbulent region of the high Reynolds number boundary layer using an atmospheric flow. J. Fluid Mech. 548, 375–402.

Lee J H, Sung H J and Krogstad P. (2011). Direct numerical simulation of the turbulent boundary layer over a cube-roughened wall. J. Fluid Mech. 669, 397–431.

Leonardi S, Orlandi P, Smalley R, Djenidi L and Antonia R. (2003). Direct numerical simulations of turbulent channel with transverse square bar on one wall. J. Fluid Mech. 491, 229–238.

Liddell B, Tucker A, Huntsman I, Manders M and McDonald C. (2001). Redesigning the Rotor Fan Blades to Improve the Cooling of Roxburgh's Hydro-Generators. 14th Australasian Fluid Mechanics Conference, Australia.

Launder B. E. and Spalding D.B (1974). The numerical computation of turbulent flows. Computer Methods in Applied Mechanics and Engineering, 3, pp. 269 –289.

Lingwood R J (1995). Absolute instability of the boundary layer on a rotating disk, J. Fluid Mech. 299, 17.

Loeb G.I, Laster D, Gracik T. (1984). The influence of microbial fouling films on hydrodynamic drag. In: Costlow JD, Tipper R (eds.) Marine Biodeterioration, an Interdiskiplinary Study. Naval Institute Press, Annapolis, Md., pp. 88–94

von Kármán T. (1946). On laminar and turbulent friction. NACA TM 1092.

Menter F R. (1994). Two-equation eddy-viscosity turbulence models for engineering applications, AIAA J., vol. 32, no. 8, pp. 1598–1605.

Mellor P H, Roberts D and Turner D R. (1991). Lumped parameter thermal model for electrical machines of TEFC design. IEE Proceedings B Electric Power Applications 138 (5), pp. 205-218.

Moody L F. (1944). Friction Factors for Pipe Flow. Trans. ASME 66, 671–688.

Moradnia P and Nilsson H. (2010). CFD of air in hydro power generators for convective cooling, using openFOAM. V European Conf on Comp Fluid Dynamics, Portugal.

Moradnia P and Nilsson H (2011). A parametric study of the air flow in an electric generator through stepwise geometry modifications. An ECCOMAS Thematic Conference, Turkey.

Moradnia P (2013). Prediction of cooling air flow in electric generators. PhD thesis, Chalmers University of Technology, Sweden.

Moradnia P, Golubev M, Chernoray V and Nilsson H. (2014). Flow of cooling air in an electric generator – An experimental and numerical study. Applied Energy 114, pp. 644-653.

Munk T. (2006). Fuel consumption through managing hull resistance. Motorship Propulsion Conference, Copenhagen.

NEED Media (2018), URL: https://need-media.smugmug.com/Graphics/Graphics/i-7cxVffp.

Nikuradse J. (1933), Strömungsgesetze in rauhen Rohren. Forsch. Arb. Ing.-Wes. No. 361.

OpenFOAM User Guide version 6, July 2018. https://openfoam.org.

Österlund (1999). Experimental Studies of Zero Pressure-gradient Turbulent Boundary Layer Flow. PhD thesis, KTH, Stockholm.

Perry A. E, Li J.D. (1990). Experimental support for the attached eddy hypothesis in zero-pressure gradient turbulent boundary layers. J. Fluid Mech. 218, pp. 405–438.

Pasha A, Hussain M and Gunubushanam N. (2010). Experimental and CFD analysis of hydrogenerator stator. 37th Int Conference on Fluid Mech and Fluid Power, India.

Pickering S J, Lampard D, Shanel M. (2001). Modelling ventilation and cooling of the rotors of salient pole machines. IEMDC 2001. IEEE Int Elect Machines and Drives Conference.

Raffel M, Willert C E, Wereley S and Kompenhans J. (2007). Particle Image Velocimetry- A Practical Guide. 2nd Edition, Ed. Springer.

Raupach M, Antonia R A and Rajagopalan S. (1991). Rough-wall turbulent boundary layers. Appl. Mech. Rev. 44, 1 –25.

Renewables First (2015). Website: http://www.renewablesfirst.co.uk/hydropower/hydropower-learning-centre/how-much-power-could-i-generate-from-a-hydro-turbine/

Rudberg P, Escobar M, Gantenbein J and Niiro N. (2015). Mitigating the adverse effects of hydropower projects: a comparative review of river restoration and hydropower regulation in Sweden and United States. Georgetown International Environmental Law Review, 27(2), 251-274.

Schrittwieser M, Marn A, Farnleitner E and Kastner G. (2014). Numerical analysis of heat transfer and flow of stator duct models. IEEE Trans on Ind Applications 50 (1), pp. 226-233.

Schlichting H. (1979). Boundary-LayerTheory. 7th ed. McGraw-Hill, NewYork, pp. 602–603

Schrittwieser M, Bíró O, Farnleitner E and Kastner G. (2015). Characterizing the convective heat transfer on stator ventilation ducts for large hydro generators with a neural network. COMPEL: The International Journal for Computation and Mathematics in Electrical and Electronic Engineering, 34 (5), pp. 1522-1536.

Sieder E and Tate G. (1936). Heat transfer and pressure drop of liquids in tubes. Industrial and Engineering Chemistry, 28, pp. 1429-1435.

Souza Mendes P. R. "The naphthalene sublimation technique." Experimental Thermal and Fluid Science 4.5 (1991): 510-523.

Taylor J L. (1960). Calculating air flow through electrical machines. Electrical Times, pp. 82-84.

Savio L, Ola Berge B, Koushan K, Axelsson M. (2015). Measurements of Added Resistance Due to Increased Roughness on Flat Plates. EU FP7 Bye-Fouling Project Report.

Schlichting H. (1979). Boundary-LayerTheory. 7th ed. McGraw-Hill, NewYork.

Schultz, M.P. (2002). The relationship between frictional resistance and roughness for surfaces smoothed by sanding. Trans. ASME 124, pp. 492–499.

Schultz, M.P. (2004). Frictional resistance of antifouling coating systems. ASME J. Fluids Eng. 126, pp. 1039–1047.

Schultz M.P, Flack K. A. (2003). Turbulent boundary layers over surfaces smoothed by sanding. J. Fluids Eng. 125 (5), pp. 863–870.

Schultz M.P., Myers A. (2003). Comparison of three roughness function determination methods. Experiments in Fluids, pp. 372–379.

Taylan, M. 2010. An Overview: Effect of Roughness and Coatings on Ship Resistance, In Proc. of Int. Conf. on Ship Drag Reduction, SMOOTH-SHIPS.

Townsin R, Byrne D, Svensen T and Milne A. (1981). Estimating the technical and economic penalties of hull and propeller roughness. Trans. SNAME 89, 295–318.

UNCTAD (2017). Review of Maritime Transport 2017. United Nations publication. New York and Geneva.

Ujiie R, Arlitt R and Etoh H. (2006). Application of computational fluid dynamics CFD on Ventilation-cooling optimization of electrical machines. Energy Technol. Gen. Transm.

Versteeg H K and Malalasekera W. (1995). Introduction to computational fluid dynamics. The finite volume method. Ed. Longman

Wallin M, Ranlöf M and Lundin U. (2010). Design and construction of a synchronous generator test setup. XIX Int Conf on Electrical Machines (ICEM 2010), Rome.

World Energy Council. World Energy Resources Hydropower, 2016.

Yuan J and Piomelli U. (2014). Estimation and prediction of the roughness function on realistic surfaces. J. Turbulence 15, 350–365.